Am J Cancer Res 2023;13(1):118-142
www.ajcr.us /ISSN:2156-6976/ajcr0146970

Original Article

NADPH oxidase 1 in chronic pancreatitis-activated pancreatic stellate cells facilitates the progression of pancreatic cancer

Ananya Chakraborty[1], Bithika Halder[1], Souravi Mondal[1], Amanda Barrett[2], Wenbo Zhi[3], Gabor Csanyi[4], Maria E Sabbatini[1]

[1]Department of Biological Sciences, Augusta University, Augusta, Georgia, USA; [2]Department of Surgical Pathology, Medical College of Georgia, Augusta University, Augusta, Georgia, USA; [3]Center for Biotechnology and Genomic Medicine, Medical College of Georgia, Augusta University, Augusta, Georgia, USA; [4]Department of Pharmacology and Toxicology, and Vascular Biology Center, Medical College of Georgia, Augusta University, Augusta, Georgia, USA

Received October 12, 2022; Accepted November 12, 2022; Epub January 15, 2023; Published January 30, 2023

Abstract: Patients suffering from chronic pancreatitis (CP) have a higher risk of pancreatic ductal adenocarcinoma (PDAC) compared to the general population. For instance, the presence of an activated pancreatic stellate cell (PaSC)-rich stroma in CP has facilitated the progression of non-invasive pancreatic intraepithelial neoplasia (PanIN) lesions to invasive PDAC. We have previously found that in a mouse model of CP, NADPH oxidase 1 (Nox1) in activated PaSCs forms fibrotic tissue and up-regulates both matrix metalloproteinase (MMP) 9 and the transcription factor Twist1. Yet, the role and mechanism of Nox1 in activated PaSCs from mice with CP (CP-activated PaSCs) in the progression of PDAC is unknown. For that, we tested the ability of Nox1 in CP-activated PaSCs to facilitate the growth of pancreatic cancer cells, and the mechanisms involved in these effects by identifying proteins in the secretome of CP-activated PaSCs whose production were Nox1-dependent. We found that, *in vitro*, Nox1 evoked a pro-invasive and cancer-promoting phenotype in CP-activated PaSCs via Twist1/MMP-9 expression, causing changes in the extracellular matrix composition. *In vivo*, Nox1 in CP-activated PaSCs facilitated tumor growth and stromal expansion. Using mass spectrometry, we identified proteins protecting from endoplasmic reticulum, oxidative and metabolic stresses in the secretome of CP-activated PaSCs whose production was Nox1-dependent, including peroxiredoxins (Prdx1 and Prdx4), and thioredoxin reductase 1. In conclusion, inhibiting the Nox1 signaling in activated PaSCs from patients with CP at early stages can reduce the reorganization of extracellular matrix, and the protection of neoplastic cells from cellular stresses, ameliorating the progression of PDAC.

Keywords: NADPH oxidase 1, MMP-9, peroxiredoxin, thioredoxin reductase 1, Twist1, pancreatic stellate cells, extracellular matrix

Introduction

The greatest risk factor associated with pancreatic ductal adenocarcinoma (PDAC) is chronic pancreatitis (CP), which is a disease characterized by long-standing inflammation that leads to irreversible destruction of the parenchyma and replacement with fibrotic tissue (i.e., stroma) [1], mainly produced by activated pancreatic stellate cells (PaSCs) [2]. For instance, the progression of non-invasive pancreatic intraepithelial neoplasia (PanIN) lesions to invasive PDAC increases with CP, amongst other factors (e.g., age) [3]. In mouse models, both the induction of CP and the expression of oncogenic *Kras* lead to a progression of PDAC [4].

The sequence of histological changes from CP to invasive PDAC starts with development of CP, followed by pancreatic atrophy, squamous metaplasia, PanIN1-2 lesions, PanIN-3 lesions (dysplasia) and invasive PDAC [5]. This transition takes about 10 years to complete and occurs in 1.1% patients with CP [6].

One of the proposed landmarks of CP that facilitates the progression of PDAC is the presence

of activated PaSC-rich stroma [7-9]. Other findings support this mechanism by showing that the ablation of PDAC-associated fibroblasts (CAFs), which are thought to arise mainly from activated PaSCs [10], suppresses tumor progression [11, 12]. For instance, unlike normal wound healing [13], in patients who have PanIN lesions, quiescent PaSCs (a non-secretory phenotype) become perpetually activated (a secretory phenotype) by pro-fibrotic factors released from PanIN lesions, which result in the progression of these lesions to invasive PDAC by releasing matrix metalloproteinases (MMPs) [7-9] from activated PaSCs [14], amongst other cells in the stroma (e.g., macrophages) [15]. Once released, MMPs degrade two histological barriers: the basal lamina (a thin layer composed of collagen IV and laminin, amongst others), and the interstitial extracellular matrix (ECM), facilitating the detachment of PanIN lesion cells from the basal lamina and their spread [16].

One barrier to progress in preventing the transition from CP to invasive PDAC is the limited knowledge regarding the mechanism by which quiescent PaSCs become activated by inflammatory mediators releasing during CP, expand, and synthesize the stroma and MMPs, facilitating the progression of PDAC. One of the inflammatory mediators of CP are reactive oxygen species (ROS) [17]. ROS generation can occur as a primary product of NADPH oxidase (Nox) enzymes. The rodent genome encodes six Nox enzymes: Nox1-4, Duox1 and Duox2 [18]. In particular, Nox1 has participated in the development of colon cancer [19], prostate cancer [20], Ras oncogene transformation of human keratinocytes [21], NIH3T3 cells [22], and normal rat kidney cells [23]. However, Nox1 participation in the progression of PDAC is still unknown.

We and other found that quiescent PaSCs become activated by ROS [24-26]. Because: i) Nox1 is expressed in PaSCs [25-27], but not in peritoneal macrophages [26], and up-regulates MMP-9 [26]; ii) activated PaSCs from mice with CP express higher levels of MMP-9 than activated PaSCs from healthy mice [26], and iii) Nox1 facilitates the invasion of Kras-transformed rat kidney fibroblast cells through MMP-9 [28], we hypothesized that activated PaSCs from mice with CP display a more pro-invasive phenotype than activated PaSCs from healthy mice in a Nox1-depedent manner. To test this hypothesis, we compared the ability of Nox1 in activated PaSCs from mice with or without CP to facilitate both the migration/invasion and the growth of pancreatic cancer cells. We also explored the mechanisms by which Nox1 facilitates these actions by identifying proteins in the secretome of activated PaSCs from mice with CP whose production were Nox1-dependent.

Materials and methods

Ethical approval

All experiments were conducted in accordance with the National Institute of Health Guidelines for the Care and Use of Laboratory Animals and approved by the Augusta University Institutional Animal Care and Use Committee (IACUC) (protocol #2017-0878).

Materials

Reagents

Caerulein (#C9026), protease (#P5147) were purchased from Sigma Aldrich (St. Louis, MO), collagenase P (11213857001), DNase I recombinant (04716728001), leupeptin and aprotinin from Roche Diagnostics (Indianapolis, IN), bovine albumin serum fraction V (BSA) from MP Biomedicals (Solon, OH), Iscove's Modified Dulbecco's medium (IMDM) and Dulbecco's minimal essential medium (DMEM)/high glucose from HyClone (Logan, Utah), protein determination reagent from Bio-Rad Life Science Research (Hercules, CA), and supersignal West Femto Chemiluminescent Substrate from Thermo Fisher Scientific (Rockford, IL). We verified the action/potency of caerulein physiologically by measuring amylase release. We observed a 3-fold increase in amylase release at 1×10^{-10} M based on previous results in the lab using cholecystokinin-8 [29].

Antibodies

Antibodies against the following proteins were used: rabbit polyclonal antibodies to collagen 1A1 (#84336), laminin gamma-1 (LAMC1) (#92921), rabbit monoclonal antibodies to calponin-1 (#17819), vimentin (#5741), α-smooth muscle actin (SMA) (#19245), thioredoxin reductase 1 (TrxR1) (#15140), connective tissue growth factor (CTGF) (#86641), protein disulfide-isomerase (PDI) (#3501), desmin (#5332),

human MMP-9 (#13667), human fibronectin (#26836), collagen 1A1 (#84336); mouse monoclonal antibodies to α-tubulin (#3873) were provided by Cell Signaling Technology (Beverly, MA); mouse monoclonal antibody against Twist1 (NBP2-37364) from Novus Biologicals (Centennial, CO); rabbit polyclonal antibody against mouse fibronectin (#AB2033) from EMD Millipore Corp (Temecula, CA), goat polyclonal antibody against mouse MMP-9 (#AF909) from R&D Systems (Minneapolis, MN), rabbit polyclonal antibody against mouse collagen IV (#2150-1470) (only used in immunohistochemistry; it did not work in Western blotting) from Bio-Rad (Hercules, CA), rabbit polyclonal antibody against human collagen IV (SAB4300752) from Sigma-Aldrich (St. Louis, MO), rat monoclonal against cytokeratin 19 (TROMA-III) from Developmental Studies Hybridoma Bank, mouse monoclonal antibody against Prdxs 1,2,4 (#sc-137222), anti-mouse IgG, horseradish peroxidase (HRP)-linked (7076) and anti-rabbit IgG, HRP-linked (7074) from Cell Signaling Technology (Beverly, MA). A representative immunoblot for each antibody showed a band at the right molecular weight. We used samples with proven presence of the protein of interest as a positive control and samples with proven absence of the protein of interest as a negative control.

Cells

We maintained and cultured HPAC and MIA PaCa-2 as recommended by American Type Culture Collection (ATCC) and as we previously published [30]. HPAC cells and MIA PaCa-2 cells were obtained from ATCC in 2018. The genotypic and phenotypic characteristics of these two pancreatic cancer cell lines can be found in [31]. All experiments were carried out between passages 5 and 20 after receipt. Cell lines were authenticated at the source. Cells were tested annually for the presence of mycoplasma (Venor™ GeM Mycoplasma Detection Kit, PCR-based; MP0025; Sigma).

Mice

C57BL/6 mice: C57BL/6 mice (*Nox1*-competent or wild type) were provided by Envigo (Indianapolis, IN).

Nox1-deficient B6.129X1-Nox1$^{tm1Kkr/J}$ (Nox1-null) mice: They were from the Jackson Laboratory as we previously published [26]. The development of *Nox1*-null mice has been previously described [32].

NSG^{TM} mice (also known as NOD.Cg-Prkdc scid IL2 rg tm1Wjl/SzJ): They were from the Jackson Laboratory. NSG^{TM} mice are most highly immunodeficient mice to be used for cancer xenograft modeling because these mice do not have mature T cells, B cells, natural killer cells, complement system, defective dendritic cells, or defective macrophages [33]. NSG^{TM} mice were maintained in a specific pathogen-free barrier facility at Augusta University.

Methods

Mouse model of CP

We divided 7-8 weeks old C57BL/6 (*Nox1*-competent) and *Nox1*-deficient B6.129X1-Nox1$^{tm1Kkr/J}$ (*Nox1*-null) mice into two groups. Mice were fasted overnight and intraperitoneally injected with 50 ug/kg caerulein 6 times hourly, three times per week for 7 weeks as previously described [34] and we have previously published [26]. The control animals received similar injections of normal saline. We dissolved caerulein in sterile saline. We euthanized mice 4 days following their final caerulein injection using carbon dioxide followed by a secondary method of euthanasia (bilateral thoracotomy).

Isolation of PaSCs

We isolated PaSCs as previously described [26]. We corroborated the identity of PaSCs by the autofluorescence of vitamin A present in cytoplasmic lipid droplets (quiescent cells) and by the presence of α-smooth muscle actin (αSMA) by immunohistochemistry (IHC) (activated cells) as previously described [2, 26]. PaSCs were cultured in 24-well plates until confluence, and, in some experiments, in 12-well plates until confluence. We changed IMDM Gluta^{Max} medium every two days.

Invasion/migration

We studied cell invasion/migration using two approaches: 1) Cytoselect^{TM} cell invasion assay kit, and 2) scratch wound migration assay.

Cytoselect^{TM} invasion transwell assays: We performed invasion transwell assays with a

CytoSelect™ cell invasion assay kit (Cell Biolabs Inc. USA) as previously done in the lab [30]. We used HPAC and MIA PaCa-2 cells because they have different grades of differentiation (HPAC cells are well differentiated, whereas MIA PaCa-2 cells are poorly differentiated [31]). Differences in grades of differentiation can cause differences in behaviors when they are co-cultured with PaSCs. We serum-starved subconfluent HPAC and MIA PaCa-2 cells overnight, detached, and plated 1.0×10^4 cells onto the transwell inserts (8.0 um pore size; Cell Biolabs Inc. USA) in serum-free media (the upper surface of the insert membrane was coated with a uniform layer of dried pseudo-model of basal membrane matrix solution that discriminate between invasive cells from non-invasive cells). Then, we placed the inserts in 24-well plates filled with medium containing 10% fetal bovine serum (FBS) containing different amount of activated PaSCs from male *Nox1*-competent or male *Nox1*-null mice with or without CP and allowed them to invade for 16 hours. We placed an insert with HPAC or MIA PaCa-2 cells (1.0×10^4 cells) in a well without PaSCs (monoculture), but filled with medium containing 10% FBS, to consider the differences in loading between experiments. We determined the absorbance at 560 nm. We then calculated the fold of increase to the absorbance of transwells with HPAC or MIA PaCa-2 cells without PaSCs. We estimated the total amount of PaSCs in the wells by isolating RNA and synthetizing complementary DNA (cDNA). We plotted fold of increase *versus* the amount of dsDNA of PaSCs. We determined the slope (mean ± SEM) using the linear regression analysis of GraphPad Prism software.

Scratch wound migration assay: We performed scratch wound migration assay as previously described [35]. We plated HPAC or MIA PaCa-2 cells (1.0×10^4 cells) in 6-well plates, allowed them to adhere and grow to confluence. Then, we created a wound using 200-ul pipette tip, added IMDM medium without serum (without conditioned media or CM) or 48-h CM of activated PaSCs from male *Nox1*-compotent mice or male *Nox1*-null mice with or without CP. We captured the images with an Olympus CK2 inverted light microscope (Olympus America, Inc., Melville, NY) with an X4 objective lens. A Canon digital SLR camera was connected to the microscope. We determined the relative wound width (in inches) over time (the length was measured using Photoshop and did not represent the actual length of a 200-ul pipette tip). We determined the rate of closure (slope ± SEM) using the linear regression analysis of GraphPad Prism software.

Changes in the gene expression of activated PaSCs from Nox1-competent and Nox1-null mice with or without CP co-cultured with HPAC or MIA PaCa-2 cells

We serum-starved subconfluent HPAC and MIA PaCa-2 cells overnight, detached, and plated 1.0×10^4 cells onto the transwell inserts in serum-free media. Then, we placed them in 24-well plates filled with medium containing 10% FBS and activated PaSCs from male *Nox1*-competent or male *Nox1*-null mice with or without CP and incubated for 16 hours. We determined the gene expression at mRNA level of PaSCs as described below.

Determination of gene expression at mRNA level

RNA isolation and RT-PCR: A small piece of mouse pancreas (40 mg) was cut and immediately placed in 1 ml of RNA*later* solution (Invitrogen by Thermo Fisher Scientific, Rockford, IL) as previously described [26]. Total RNA was isolated from mouse pancreas using Trizol and RNeasy® Mini kit (Qiagen, Inc. USA, Valencia, CA). Total RNA from PaSCs was isolated using RNeasy® Mini kit as previously described [26]. First-strand complementary DNA was synthesized with TaqMan Reverse Transcription Reagents (Thermo Fisher Scientific, Waltham, MA). Four μg of cDNA was used in each regular PCR reaction. Amplification was done with Taq DNA polymerase from Expand High Fidelity Enzyme System (Roche Diagnostics, Indianapolis, IN). The PCR primers were listed in **Table 1**. The efficiency of the primers was checked beforehand by using control DNA provided by GeneCopoeia, Inc.

Real-time quantitative PCR: The relative expression of genes in PaSCs from *Nox1*-compotent mice or *Nox1*-null mice with or without CP was evaluated by real-time quantitative PCR analysis using Absolute Blue SYBR Green ROX mix (Thermo Fisher Scientific) and a real-time quantitative PCR machine (LightCycler 96 system, Roche) as previously described [26].

Table 1. Primers used for analysis of mRNA expression using regular PCR and real-time quantitative PCR

Gene (*specie: mus musculus*)	Forward Primer (5' to 3')	Reverse Primer (5' to 3')	Accession Number	PCR product size
NADPH oxidase 1	GTTTCTCTCCCGAAGGACCTC	TTCAGCCCCAACCAGGAAAC	NM_172203.2	136 bp
thioredoxin reductase 1 (TXNRD1)	GTCACACCGACTCCTCTTGG	AGTTGCGCGAGTCTTTCAGA	AB027565.1	127 bp
Calponin-1 (CNN1)	CCTACGGCTTGTCTGCTGAA	CTGTCACCCCCTCAATCCAC	NM_009922.4	96 bp
Connective tissue growth factor (CTGF) (CCN2)	AGAACTGTGTACGGAGCGTG	GTGCACCATCTTTGGCAGTG	NM_010217.2	110 bp
transglutaminase 2 (TGM2)	AGAGTGTCGTCTCCTGCTCT	GTAGGGATCCAGGGTCAGGT	NM_009373.3	100 bp
heat shock protein 4 (HSPA4)	TCAGAGCTGCTATGTCGCTG	CAGCGGTCGCTATACTCGTT	NM_008300.3	72 bp
insulin-like growth factor binding protein 2 (IGFBP2)	CACTACCGTTGCCCACAAGC	CAGCAGCAAGAGCAACGACG	BC054473.1	87 bp
Peroxiredoxin 1	CACCCAAGAAACAAGGAGGA	AAAAAGGCCCCTGAAAGAGA	NM_011034.4	125 bp
Peroxiredoxin 2	GGTGCCTTCAAGGAAATCAA	GCCTAGCTTTCGGAAGTCCT	BC086783.1	141 bp
Peroxiredoxin 3	TCGTCAAGCACCTGAGTGTC	GACTTCTCCATGGGTCTCCA	NM_007452.2	104 bp
Peroxiredoxin 4	AGTGCCACTTCTACGCTGGT	TTGGAGATCTTGGCTTTGCT	BC019578.1	100 bp
Peroxiredoxin 5	ACCGGGAAAGAAGGTGAACT	GGCAGGTGGGTCTTAGAACA	AF110733.1	105 bp
Peroxiredoxin 6	CCTGGAGCAAGGACATCAAT	CCAAAATGAACACCACACG	NM_007453.4	171 bp
collagen, type I, alpha 1 (Col1a1)	ACGTGGAAACCCGAGGTATG	GGGTCCCTCGACTCCTACAT	NM_007742.4	183 bp
Collagen IV, alpha 1 (Col4a1)	AGATTCCGCAGTGCCCTAAC	CGATGAATGGGGCGCTTCTA	NM_009931.2	147 bp
Fibronectin	CCAAGACCATACCTGCCGAA	AGGCCCGGAACATGAGGATA	NM_010233.2	98 bp
Laminin subunit gamma-1 (Lamc1)	AGCCGACTGCAGAATATCCG	CCCTGGAGGCGATCTCAATC	NM_010683.2	109 bp
Interleukin-6 (IL-6)	GAGTCACAGAAGGAGTGGCT	AACGCACTAGGTTTGCCGA	NM_031168.2	108 bp
α-smooth muscle actin	TGACTCACAACGTGCCTATC	CTCGGCAGTAGTCACGAAGG	NM_007392.3	140 bp
Matrix metalloproteinase 9 (MMP-9)	TCAAAGGCCTCAAGTGGGAC	TCATCGATCATGTCTCGCGG	NM_013599.4	85 bp
Genes mediating EMT				
Twist basic helix-loop-helix transcription factor 1 (twist1) [26]	ATTCAGACCCTCAAACTGGCG	TCTTGGAGTCCAGCTCGTCG	NM_011658.2	79 bp
Snail family zinc finger 1 (Snail) [26]	ACCTCCAAACCCACTCGGAT	GACATGCGGGAGAAGGTTCG	NM_011427.3	69 bp
Housekeeping gene				
18S rRNA [26]	GTAACCCGTTGAACCCCATT	CCATCCAATCGGTAGTAGCG	NR_003278.3	150 bp

Primers were designed with NIH primer blast (https://www.ncbi.nlm.nih.gov/tools/primer-blast) based on genes sequences obtained from the Gen Bank NCBI sequence Viewer.

Two μg of cDNA was used in each reaction. The PCR primers were listed in **Table 1**. Results from real-time quantitative PCR were evaluated using the $2^{-\Delta\Delta Cq}$ method as previously described [36]. 18S rRNA was used as a reference. We verified the amplification efficiency of each primer by making dilution series from mouse pancreas and analyzing the slope of the calibration curve for each primer using qPCR as previously described [30]. We only used primers showing efficiencies between 90 and 100% (-3.6≥ slope ≥3.3).

Determination of gene expression at protein level

Western blotting analysis was carried out as previously described [26, 30]. Immunodetection of proteins was carried out using sodium dodecyl sulfate (SDS)-polyacrylamide gel. Proteins in the gel were transferred to a nitrocellulose membrane (Bio-Rad Laboratories, Inc.). The membrane was blocked in 5% nonfat milk dissolved in Tris-buffered saline containing 0.1% (v/v) Tween X-20 (TBST) for 1 h at room temperature. Corresponding primary antibodies were diluted 1:1000 in 5% bovine serum albumin (BSA), and the membrane was incubated with the antibody overnight at 4°C followed by treatment with a HRP-conjugated secondary antibody (1:5000 in 5% nonfat milk) for 1 h at room temperature. After washing with TBST, peroxidase activity was visualized using the SuperSignal West Femto sensitivity substrate kit (Thermo Fisher Scientific, Waltham, MA). Images were taken using Foto/Analyst Luminary FX Imaging Workstation (Fotodyne Incorporated, Hartland, WI). *Quantification:* The quantitative analysis was performed using density analysis software from TotalLab Quant TL100 (Newcastle upon Tyne, UK). The density of each band was measured and the result was normalized to its loading control (e.g., tubulin) by dividing the integrated density volume (IDV) by the IDV of loading control to account for differences in loaded amounts.

MIA PaCa-2 cells and PaSCs co-transplantation

To evaluate the effect of Nox1 in activated PaSCs from mice with CP on tumor growth *in vivo*, we anesthetized NSG™ mice with isoflurane, and made a small abdominal incision in the left flank and located the distal pancreas with sterile gauze. We injected into the distal pancreas of NSG™ mouse using a sterile insulin syringe (Monoject 1 ml permanent needle; 28Gx1/2) a mixture (50 ul in IMDM) of MIA PaCa-2 cells (1×10^4) with or without activated PaSCs (5×10^4) from *Nox1*-competent mice with CP or activated PaSCs (5×10^4) from *Nox1*-null mice with CP (1:5 tumor cells-to-stromal cells ratio). We used this ratio because, in cases in which an intense desmoplastic reaction is present, PaSCs in the stromal compartment greatly outnumbers the amount of neoplastic epithelial cells present in the tumor [7]. As a control, we injected activated PaSCs (5×10^4 cells/50 ul) from either *Nox1*-competent mice with CP or *Nox1*-null mice with CP alone or MIA PaCa-2 cells (1×10^4) alone to the distal pancreas of NSG™ mice. We closed the muscle and skin incisions separately: we closed the muscle layer with sutures and the skin layer with wound clips using the Autoclip Physicians Kit (Dickinson Primary Care Diagnostics Inc.). We removed the wound clips 7 days after surgery. Mice were housed in a Biosafety Level 2 (BSL-2) facility. We euthanized mice 6 weeks post-surgery to assess tumor size.

Pancreas weight/body weight (PW/BW) ratio

The body and pancreas weights were recorded when harvested and reported as PW/BW ratio.

Histology

Pancreatic tissue was fixed with 10% formalin and embedded in paraffin as previously described [26, 37]. Hematoxylin and eosin (H&E) staining was performed at the Augusta University Histology Core. Images were captured with an Olympus BX43 Bright field microscope and a Zeiss Axiovert 200 Inverted Fluorescence Phase Contrast Microscope. *Quantification:* The area of each tumor (the number of pixels quantified in the image were converted to um^2) was blinded measured using density analysis software from TotalLab Quant TL100 (analysis toolbox) (Newcastle upon Tyne, UK).

Immunohistochemistry (IHC)

IHC for mouse collagen IV in whole pancreas: Positive cells were visualized using 3,3-diaminobenzidine tetrahydrochloride (DAB) as a chromogen (color: brown) as previously described [26]. Briefly, slides were incubated first with blocking buffer (3% BSA in PBS with 0.05% Tween-20) for 1 hour at room temperature and

then with antibody against mouse collagen IV overnight at 4°C. Slides were washed with PBS with 0.05% Tween-20 and incubated with HRP-labeled secondary antibody for 30 min. After washing, the DAB solution was added to the slides, incubated for 10 min, and then washed again. The slides were mounted and a coverslip was added to the section. Images were captured with an Olympus BX43 Bright field microscope and a Zeiss Axiovert 200 Inverted Fluorescence Phase Contrast Microscope.

IHC for collagen I and III in whole pancreas (Masson's trichrome staining): Slides were deparaffinized and hydrated with distilled water, then placed in Bouin's solution for 1 hour at 56°C, washed in running tap water for 3-5 min, stained in Weigert's iron hematoxylin working solution, rinsed in running tap water for 5 min, stained in Biebrich scarlet-acid fuchsin solution for 5 min, washed in distilled water for 30 secs, differentiated in phosphomolybdic-phosphotungstic acid solution for 5 min, transferred directly (without rinse) to aniline blue solution and stained for 10 min. Slides were placed in 1% acetic acid solution for 1 min, washed in distilled water for 30 secs, dehydrated through 2 changes of anhydrous alcohol, for 1 min, cleared in 3 changes of xylene for 1 min each and mounted with resinous mounting medium. Images were captured with an Olympus BX43 Bright field microscope and a Zeiss Axiovert 200 Inverted Fluorescence Phase Contrast Microscope.

Quantification: The intensity score (IS) was blinded evaluated by comparing the staining of collagens in the surrounding stroma and graded 0 for no staining (completely negative or extremely faint), 1 for evident staining (definitely positive, but weaker than that in basement membrane) and 2 for staining stronger than 1 (similar than that in basement membrane). The proportional score was graded 0 for staining in <5% of area, 1 for staining in ≥5%, but <30% of area, 2 for staining in ≥30% of the area, but <70% of area, and 3 for staining in ≥70% of area. The final score (FS) was calculated and graded as IS × PS as previously described [38].

Liquid chromatography with tandem mass spectrometry (LC-MS/MS) analysis

We isolated PaSCs from mice with CP as previously described [26], placed them in the wells of a 24-well plate and cultured them in a serum-free IMDM medium because FBS interferes with the mass spectroscopy analysis. After 48 h, we collected the serum-free CM, centrifuged at 1000 rpm for 5 min and stored the supernatants at -80°C. We used serum-free IMDM medium as a negative control. Digested peptide samples were analyzed on an Orbitrap Fusion tribrid mass spectrometer (Thermo Scientific), to which an Ultimate 3000 nano-UPLC system (Thermo Scientific, Waltham, MA) was connected at the upfront. Two microliters of peptide sample was first trapped on a Pepmap100 C18 peptide trap (5 um, 0.3 × 5 mm, Thermo Scientific, Waltham, MA) and then washed at 20 ul/min using 2% acetonitrile with 0.1% formic acid for 10 minutes. Next, the cleaned peptides were washed off the trap and further separated on a Pepman 100 RSLC C18 column (2.0 um, 75-μm × 150-mm, Thermo Scientific, Waltham, MA) at 40°C using a gradient of between 2% to 40% acetonitrile with 0.1% formic acid over 100 min at a flow rate of 300 nl/min. LC-MS/MS analyses were performed using data-dependent acquisition in positive mode with the Orbitrap MS analyzer for precursor scans at 120,000 FWHM from 300 to 1500 m/z and the ion-trap MS analyzer for MS/MS scans at top-speed mode (3-second cycle time). Collision-induced dissociation method was used to fragment the precursor peptides with a normalized energy level of 30%. Raw MS and MS/MS spectrum for each sample were filtered and processed using the Proteome Discoverer software (v1.4, Thermo Scientific, Waltham, MA) and then submitted to SequestHT search algorithm against the Uniprot human database (10 ppm precursor ion mass tolerance: 10 ppm, product ion mass tolerance: 0.6 Da, static Carbamidomethylation of +57.021 Da). Perculator peptide spectrum matching (PSM) validator algorithm was used for peptide spectrum matching validation and false discovery rate estimation. Proteins whose subcellular location is extracellular matrix/extracellular space/basement membrane/basal lamina and/or secreted proteins were studied. Using normalized spectral counts (label-free quantification) assigned to statistically significant, *Nox1*-competent/*Nox1*-null mice predominant ratios were computed to highlight the predominance in CM of activated PaSCs from *Nox1*-competent mice with CP. We focused on proteins that were at least 2.5-fold more abundant in CM of PaSCs from *Nox1*-competent mice

with CP (cut off: 2.5-fold change) and their standard error of the mean (SEM) were lower than 10% of fold change (mean).

Statistical analysis

Results were expressed as mean ± SEM. We analyzed data using one-way repeated measures analysis of variance (ANOVA) followed by Student-Newman-Keuls post hoc tests for comparisons between multiple groups or unpaired *t*-test for comparisons between two unrelated/independent groups using Instat Graphpad software (La Jolla, CA). $P<0.05$ was considered to be the minimal level of statistical significance.

Results

In vitro studies

Nox1 in activated PaSCs from mice with CP facilitates the invasion of HPAC and MIA PaCa-2 cells

Cell invasion assay (basal lamina): We co-cultured activated PaSCs with HPAC or MIA PaCa-2 cells. In the presence of an increasing number of activated PaSCs from male *Nox1*-competent (wild type or WT) mice with CP (CP-activated PaSCs), the invasion of MIA PaCa-2 and HPAC cells increased, while the lack of Nox1 in PaSCs reduced the effect (**Figure 1A-D**). In the presence of activated PaSCs from either male healthy *Nox1*-competent or *Nox1*-null mice (the activation of these cells occurs by the treatment of a culture dish and takes 48 h [2]), no significant increase in cell invasion was observed (**Figure 1A-D**).

The co-culture of activated PaSCs from mice with CP and pancreatic cancer cell lines increases the expression of MMP-9 and Twist1 via Nox1. As we previously found [26], the induction of CP increased the expression of MMP-9 and the transcriptional repressor of E-cadherin Twist1 in activated PaSCs from male *Nox1*-competent mice with CP, and the lack of Nox1 reduced these effects (**Figures 1E** and **3**). We found that the presence of HPAC and Mia-PaCa-2 cells strengthens the ability of activated PaSCs from mice with CP to up-regulate Twist1 and MMP-9. The lack of Nox1 in activated PaSCs reduced that effect (**Figure 1E**). No changes were observed in mRNA level of transcription factor Snail as previously shown [26].

Scratch wound migration assay: In the presence of CM of activated PaSCs from male *Nox1*-competent mice with CP, the wound closed faster than in the presence of IMDM (control media) or CM of activated PaSCs from male healthy *Nox1*-competent mice (**Figure 2A-D**). The lack of Nox1 in activated PaSCs impaired the effect (**Figure 2A-D**).

The genetic deletion of Nox1 in activated PaSCs from mice with CP causes changes in their gene expression

The induction of CP increases αSMA, but not IL-6, in activated PaSCs: Using qPCR, we found that activated PaSCs from mice with CP displayed higher mRNA level of αSMA than activated PaSCs from healthy mice, without affecting the mRNA level of IL-6 (**Figure 3**). The lack of Nox1 did not alter CP-induced αSMA expression (**Figure 3**).

The deletion of Nox1 alters the expression of histological barrier proteins: Using qPCR, we found that the induction of CP increased the expression of fibronectin and, to a lesser extent, collagen I in activated PaSCs from male and female *Nox1*-competent mice (**Figure 3**). Both LAMC1 and Collagen IV were still being produced by activated PaSCs even during CP-induced healing process (**Figure 3**). The genetic deletion of *Nox1* in activated PaSCs from mice with CP reduced the expression of genes (**Figure 3**).

In vivo studies

Nox1 in activated PaSCs from mice with CP facilitates the tumor growth and the stromal expansion in an orthotopic xenograft model of PDAC

Because activated PaSCs from healthy mice did not facilitate the migration/invasion of HPAC and MIA PaCa-2 cells to the same extent as activated PaSCs from mice with CP, we then tested the ability of Nox1 in activated PaSCs from mice with CP to facilitate the growth of pancreatic cancer cells in an orthotopic xenograft model of PDAC. For that, we injected MIA PaCa-2 cells, but not HPAC cells, because MIA PaCa-2 cells are more tumorigenic than HPAC cells [31].

The main source of Nox1 in this model was activated PaSCs because, using reverse tran-

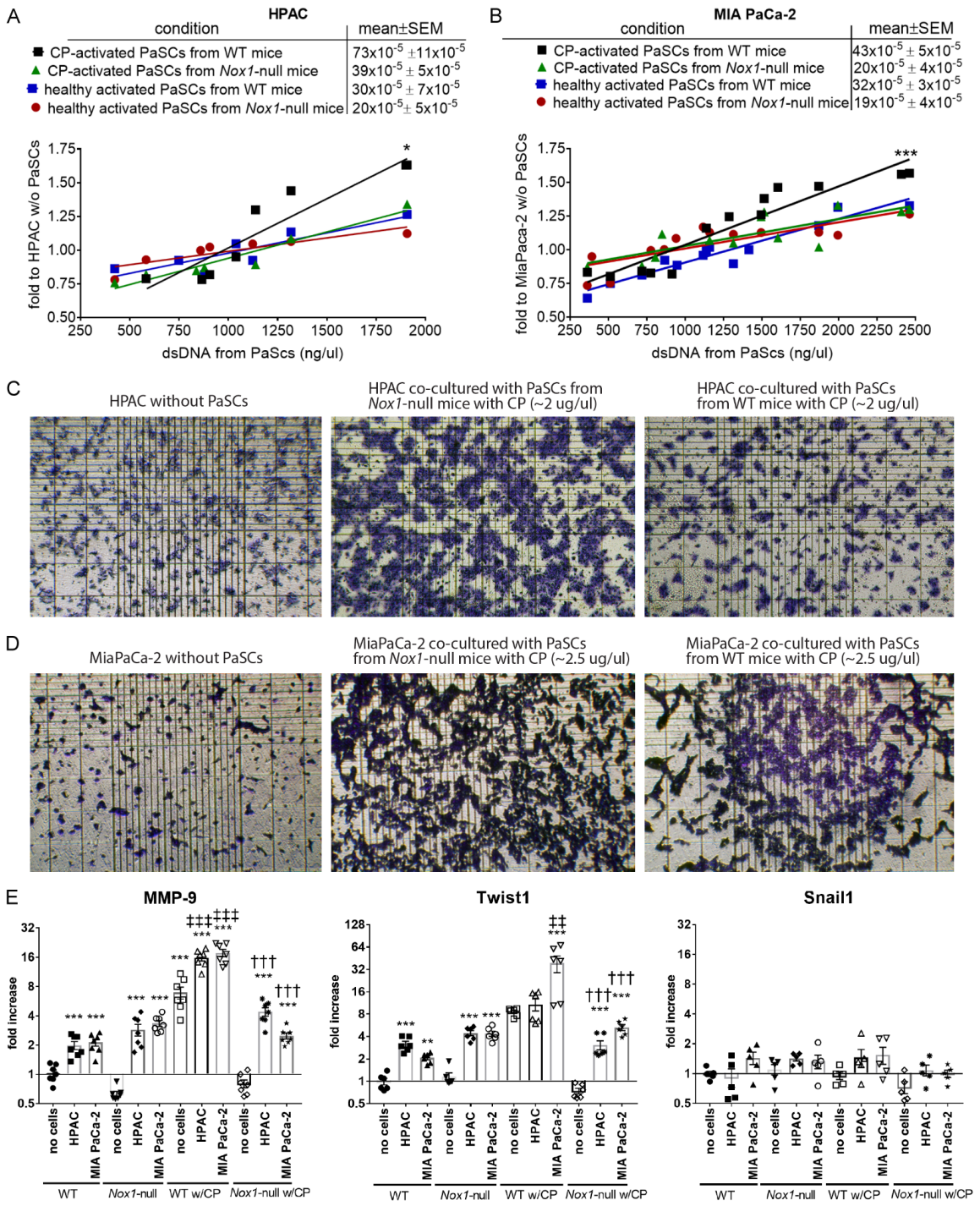

Figure 1. Nox1 in activated PaSCs from mice with CP facilitates the invasion of HPAC and MIA PaCa-2 cells. Above: We performed invasion transwell assays with a CytoSelect™ cell invasion assay kit (Cell Biolabs Inc. USA) as previously done in the lab [30] using HPAC (A) and MIA PaCa-2 (B) cells. We determined the absorbance at 560 nm and calculated the fold to the absorbance of transwells with pancreatic cancer cell lines without PaSCs. Using the linear regression analysis of GraphPad Prism software, we determined the slope (mean ± SEM). Below: Representative images of inserts showing invasive HPAC (C) or MIA PaCa-2 (D) cells. Images were taken with an Olympus CK2 inverted light microscope (Olympus America, Inc., Melville, NY) with an X4 objective lens. A Canon digital SLR camera was connected to the microscope. *Statistical Analysis:* One-way ANOVA followed by Student-Newman-Keuls post hoc performed by Instat Graphpad software (La Jolla, CA). *: P<0.05 and ***: P<0.001 *versus* activated PaSCs from *Nox1*-null mice without CP (healthy mice). n: HPAC cells: independent activated PaSCs from male WT mice with CP: 8 mice; independent activated PaSCs from male *Nox1*-null mice with CP: 7 mice; independent activated PaSCs from

healthy male WT mice: 7 mice; independent activated PaSCs from healthy male *Nox1*-null mice: 7 mice. MIA PaCa-2 cells: independent activated PaSCs from male WT mice with CP: 14 mice; independent activated PaSCs from male *Nox1*-null mice with CP: 13 mice; independent activated PaSCs from healthy male WT mice: 13 mice; independent activated PaSCs from healthy male *Nox1*-null mice: 13 mice. (E) Changes in the gene expression of activated PaSCs from *Nox1*-competent and *Nox1*-null mice co-cultured +/- HPAC and MIA PaCa-2 cells. Data were expressed as fold change in gene expression relative to male WT mice (mean ± SEM). 18s rRNA was used as a reference. *Statistical Analysis:* Two-way ANOVA followed by Student-Newman-Keuls post hoc was performed by Instat Graphpad software (La Jolla, CA). **: P<0.01 and ***: P<0.001 *vs* WT mice; ‡‡: P<0.01, and ‡‡‡: P<0.001 *vs* WT mice with CP without cancer cells. †††: P<0.001 *vs Nox1*-null mice with *CP* without cancer cells. n: MMP-9: 7 mice each group; Twist1: 6 mice each group; Snail1: 5 mice each group. WT: *Nox1*-competent mice.

scription (RT)-PCR, we found that Nox1 is not expressed in MIA PaCa-2 cells (**Figure 4A**), while it is expressed in PaSCs [25-27]. The expression of Nox1 was also evaluated in other two pancreatic cancer cells, HPAC and PANC1. None of those cells expressed Nox1 (**Figure 4A**).

Tumor growth: We observed a significant increased tumor growth (shown as pancreas weight/body weight (PW/BW) ratio) in the pancreas of male NSG™ mice co-injected with MIA PaCa-2 and activated PaSCs from male *Nox1*-competent mice with CP. We did not see tumor growth in the pancreas of NSG™ mice co-injected with MIA PaCa-2 and activated PaSCs from male *Nox1*-null mice with CP (**Figure 4B**). No tumors developed when NSG™ mice were injected with activated PaSCs from male *Nox1*-competent mice with CP into the pancreas alone (**Figure 4B**).

Fibronectin, collagen IA, αSMA and vimentin: We observed an expansion of the stromal compartment when activated PaSCs from male *Nox1*-competent mice with CP were co-injected with MIA PaCa-2 cells by studying fibronectin, collagen IA, αSMA and vimentin using qPCR (**Figure 4C**) and Western blotting (**Figure 4D**). The stromal expansion was absent when MIA PaCa-2 cells and activated PaSCs from male *Nox1*-null mice with CP were co-injected (**Figure 4C** and **4D**). No changes in the expression of studied genes were observed when male NSG™ mice were injected with activated PaSCs from male *Nox1*-competent mice with CP into the pancreas alone (**Figure 4C**).

Desmin and Keratin 19: Unlike the intermediate filament vimentin, the intermediate filaments desmin and keratin 19 decreased in the pancreas of male NSG™ mice co-injected with MIA PaCa-2 and activated PaSCs from male *Nox1*-competent mice with CP (**Figure 4D**). To test whether the lower levels of both desmin and keratin 19 in the pancreas of those mice was due to a higher MIA PaCa-2 cell population, we determined the presence of desmin and keratin 19 in MIA PaCa-2 cells and in other two pancreatic cancer cell lines: HPAC and PANC-1. Because MIA PaCa-2 cells do not express either keratin-19 or desmin (**Figure 4E**), we concluded that Nox1 in activated PaSCs from mice with CP contributed to a higher MIA PaCa-2 cell population (a bigger tumor formation) in an orthotopic xenograft model of PDAC.

Collagen IV and LAMC1: Collagen IV and LAMC1 at mRNA and protein levels increased in pancreas from male NSG™ mice co-injected with MIA PaCa-2 cells and activated PaSCs from male *Nox1*-competent mice with CP (**Figure 4C** and **4D**). The absence of Nox1 in activated PaSCs co-injected with MIA PaCa-2 cells into the pancreas of NSG™ mice prevented the up-regulation. No changes in the expression of collagen IV and LAMC1 were observed when male NSG™ mice were injected with PaSCs from male *Nox1*-competent mice with CP into the pancreas alone (**Figure 4C** and **4D**).

IL-6 and Twist1: Using qPCR (**Figure 4C**), we found that both IL-6 and Twist1 at mRNA level were up-regulated in the pancreas from male NSG™ mice injected with MIA PaCa-2 cells alone compared to male NSG™ control mice. The co-injection of MIA PaCa-2 cells and activated PaSCs from male *Nox1*-competent mice with CP into the pancreas of NSG™ mice increased even more the expression of IL-6 and Twist1. The lack of Nox1 in activated PaSCs reduced the expression of studied genes. No changes in the expression of studied genes were observed when NSG™ mice were injected with PaSCs from *Nox1*-competent mice with CP into the pancreas alone (**Figure 4C**).

MMP-9: MMP-9 at mRNA and protein levels increased in the pancreas of male NSG™ mice when activated PaSCs from male *Nox1*-com-

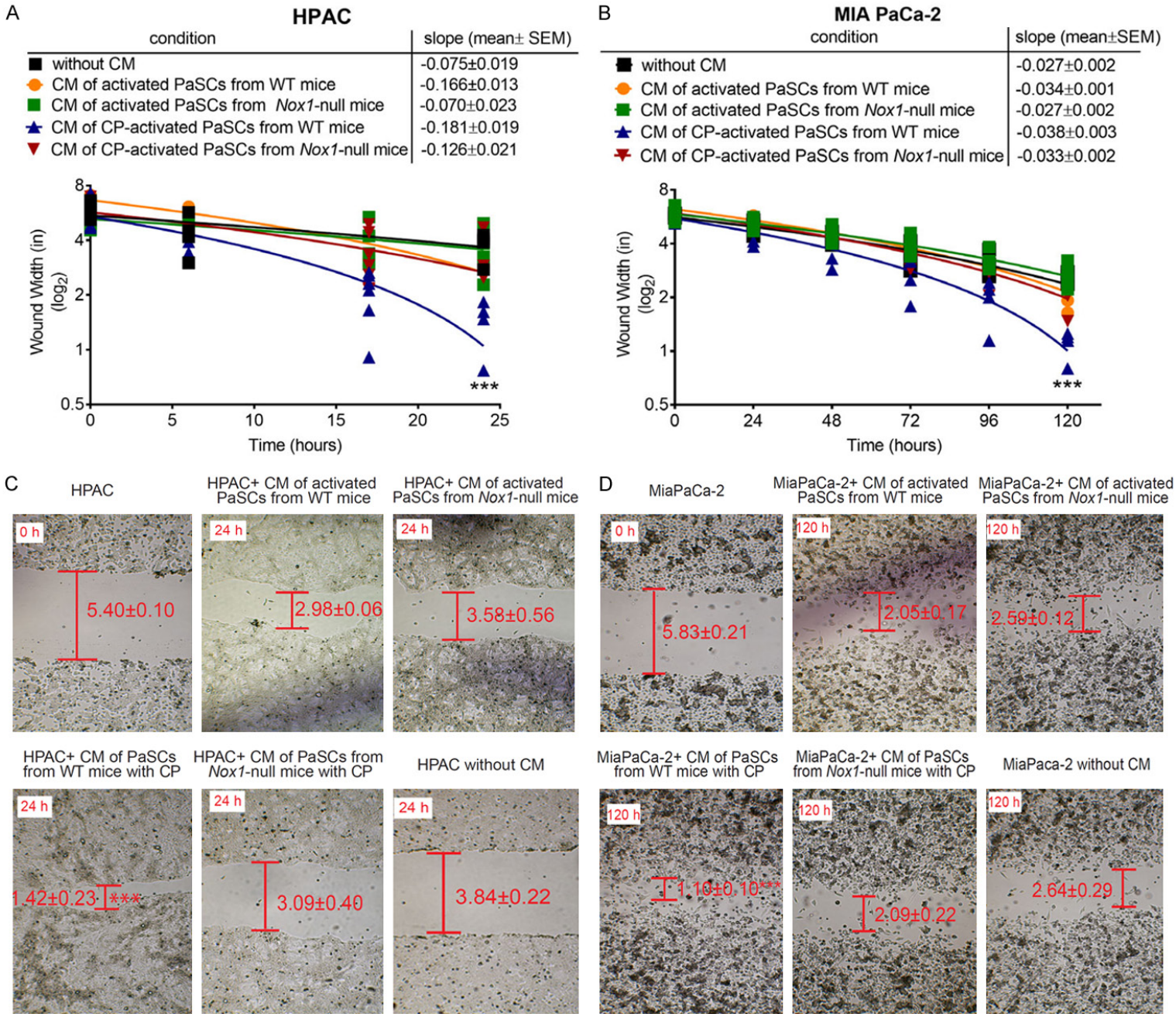
A
HPAC
condition
slope (mean± SEM)
without CM
-0.075±0.019
CM of activated PaSCs from WT mice
-0.166±0.013
CM of activated PaSCs from Nox1-null mice
-0.070±0.023
CM of CP-activated PaSCs from WT mice
-0.181±0.019
CM of CP-activated PaSCs from Nox1-null mice
-0.126±0.021
Wound Width (in) (log2)
Time (hours)
***
B
MIA PaCa-2
condition
slope (mean±SEM)
without CM
-0.027±0.002
CM of activated PaSCs from WT mice
-0.034±0.001
CM of activated PaSCs from Nox1-null mice
-0.027±0.002
CM of CP-activated PaSCs from WT mice
-0.038±0.003
CM of CP-activated PaSCs from Nox1-null mice
-0.033±0.002
Wound Width (in) (log2)
Time (hours)
***
C
HPAC
HPAC+ CM of activated PaSCs from WT mice
HPAC+ CM of activated PaSCs from Nox1-null mice
0 h
5.40±0.10
24 h
2.98±0.06
24 h
3.58±0.56
HPAC+ CM of PaSCs from WT mice with CP
HPAC+ CM of PaSCs from Nox1-null mice with CP
HPAC without CM
24 h
1.42±0.23***
24 h
3.09±0.40
24 h
3.84±0.22
D
MiaPaCa-2
MiaPaCa-2+ CM of activated PaSCs from WT mice
MiaPaCa-2+ CM of activated PaSCs from Nox1-null mice
0 h
5.83±0.21
120 h
2.05±0.17
120 h
2.59±0.12
MiaPaCa-2+ CM of PaSCs from WT mice with CP
MiaPaCa-2+ CM of PaSCs from Nox1-null mice with CP
MiaPaca-2 without CM
120 h
1.10±0.10***
120 h
2.09±0.22
120 h
2.64±0.29

Figure 2. Nox1 in activated PaSCs from mice with CP facilitates the migration of HPAC and MIA PaCa-2 cells. We plated HPAC (A) or MIA PaCa-2 (B) cells (1.0×10^4 cells), allowed them to adhere and grow to confluence. Then, we created a wound using 200-ul pipette tip, added IMDM medium with 10% FBS (without conditioned media), 24-h conditioned media (CM) of activated PaSCs from male *Nox1*-compotent (WT) mice or male *Nox1*-null mice with or without CP. We determined the relative wound width (in inches) over time (the length was measured using Photoshop). Using the linear regression analysis of GraphPad Prism software, we determined the rate of closure (slope ± SEM). (C and D) Representative images were taken (C: HPAC cells; D: MIA PaCa-2 cells). We captured the images with an Olympus CK2 inverted light microscope (Olympus America, Inc., Melville, NY) with an X4 objective lens. A Canon digital SLR camera was connected to the microscope. *Statistical Analysis:* One-way ANOVA followed by Student-Newman-Keuls post hoc performed by Instat Graphpad software (La Jolla, CA). ***: P<0.001 *versus* HPAC or MIA PaCa-2 cells without CM (IMDM medium with 10% FBS). n: HPAC cells: control (without conditioned media): 6 independent experiments; independent activated PaSCs from male WT mice with CP: 6 mice; independent activated PaSCs from male *Nox1*-null mice with CP: 7 mice; independent activated PaSCs from healthy male WT mice: 5 mice; independent activated PaSCs from healthy male *Nox1*-null mice: 5 mice; MIA PaCa-2 cells: control (without conditioned media): 5 independent experiments; independent activated PaSCs from male WT mice with CP: 5 mice; independent activated PaSCs from male *Nox1*-null mice with CP: 5 mice; independent activated PaSCs from healthy male WT mice: 5 mice; independent activated PaSCs from healthy male *Nox1*-null mice: 5 mice.

petent mice with CP were co-injected with MIA PaCa-2 cells. MMP-9 lowered in the pancreas of NSG™ mice co-injected with activated PaSCs from male *Nox1*-null mice with CP and MIA PaCa-2 cells (**Figure 4C** and **4D**).

Hematoxylin and eosin (H&E) and Masson's trichrome staining: Based on the histopathologic analysis, the invasive malignant focuses in all of these tissues were poorly differentiated, had a very prominent rhabdoid morphology (eccentric, eosinophilic cytoplasm) and did not show abundant desmoplastic stroma. The tumor in the pancreas co-injected with MIA PaCa-2 cells and activated PaSCs from male *Nox1*-competent mice with CP had the most infiltrative appearance at the borders, while the others have more circumscribed borders (**Figure 5A**: H&E, **Figure 5B**: Masson's trichrome).

Mouse fibroblasts are the sources of collagen IV in the orthotopic xenograft model of PDAC

To determine the source of mouse collagen IV in the orthotopic xenograft model of PDAC, we carried out IHC using a mouse collagen IV antibody. We found that in the pancreas from male NSG™ mice (control), mouse collagen IV was present in the basement membrane around acini (a strong periacinar staining) and around blood vessels (a strong perivascular staining). When we transplanted MIA PaCa-2 cells into the pancreas of male NSG™ mice, collagen IV was present around blood vessels (strong perivascular staining) and fibroblasts (a weak staining). The co-injection with MIA PaCa-2 cells and activated PaSCs from male *Nox1*-competent mice with CP increased even more the staining of collagen IV due to a higher number of blood vessels and fibroblasts. The co-injection with MIA PaCa-2 cells and activated PaSCs from male *Nox1*-null mice with CP displayed an immunostaining similar to control mice (i.e., periacinar and perivascular staining) (**Figure 5C**).

Proteomic studies

Using mass spectrometry, we further discovered proteins in the secretome of activated PaSCs from mice with CP, whose production was Nox1-dependent. We did not analyze the secretome of activated PaSCs from healthy mice because they were not as pro-invasive as those cells from mice with CP.

Overall, a total of 104 proteins were identified in the CM across the ten samples (5 CM of PaSCs from male *Nox1*-competent mice with CP, 5 CM of PaSCs from male *Nox1*-null mice with CP) and analyzed. After normalizing the protein abundances and calculating the *Nox1*-competent mice and *Nox1*-null mice ratios, a total of 11 proteins had a ratio greater than 2.5 (**Table 2**). The mass spectrometry proteomics data have been deposited to the ProteomeXchange Consortium via the PRIDE partner repository [39] with the dataset identifier PXD034177.

Nox1 in activated PaSCs from mice with CP induces the production of a number of chaperones protecting cancer cells from endoplasmic reticulum (ER) stress

Including Heat shock 70 kDa protein 4 (gene: *Hspa4*; fold change: 12.13±0.99), Heat shock cognate 71 kDa protein (gene: *Hspa8*; fold change: 4.02±0.41), Heat shock protein HSP

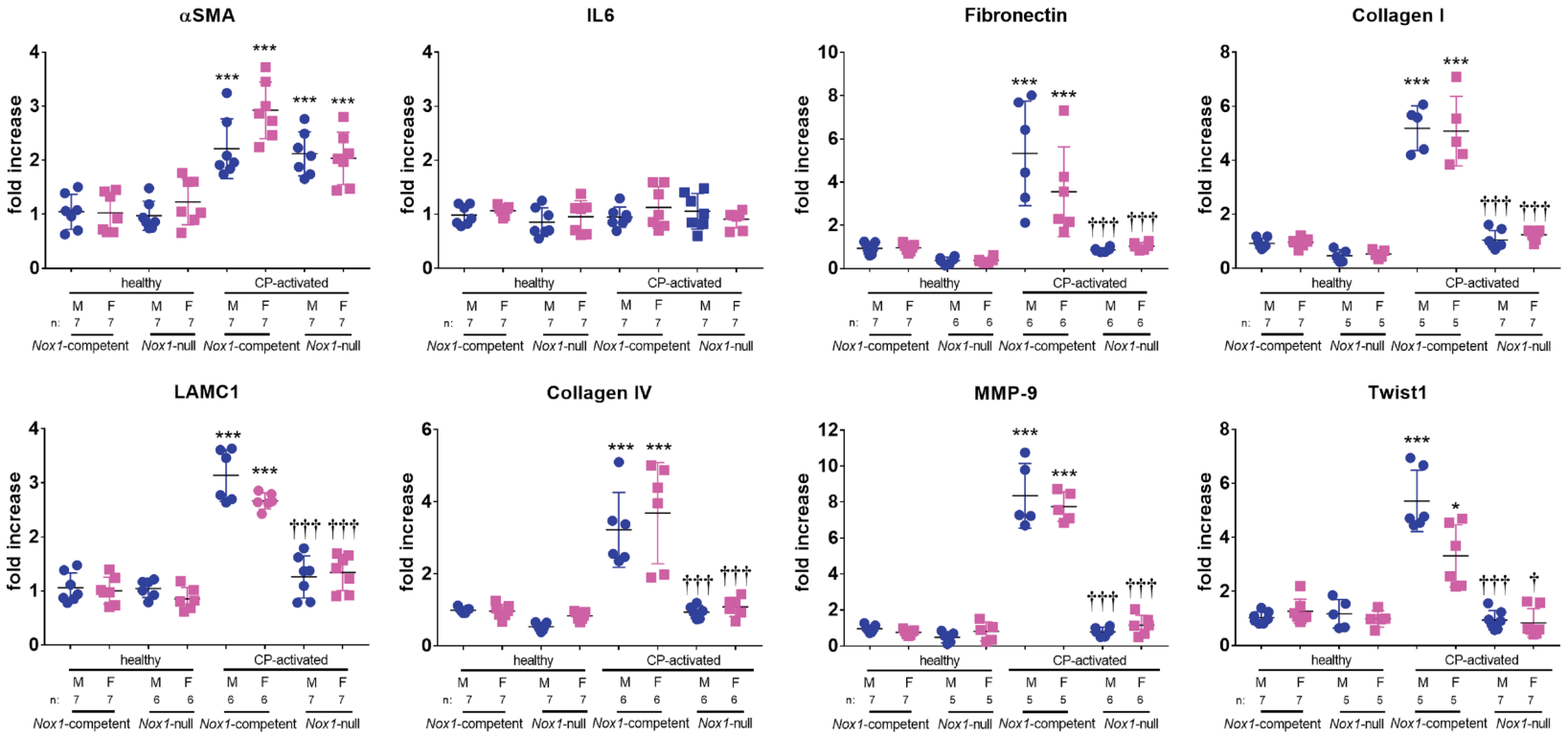

Figure 3. The absence of Nox1 reduces a number of PaSC-produced proteins following induction of CP. Data were expressed as fold change in gene expression relative to PaSCs from *Nox1*-compentent healthy mice (male or female) (mean ± SEM). 18S rRNA was used as a reference. *Statistical Analysis:* One-way ANOVA followed by Student-Newman-Keuls post hoc performed by Instat Graphpad software (La Jolla, CA). ***: P<0.001 *vs* WT mice; †††: P<0.001 *vs* WT mice with CP. n: as indicated in the figure. WT: *Nox1*-competent mice.

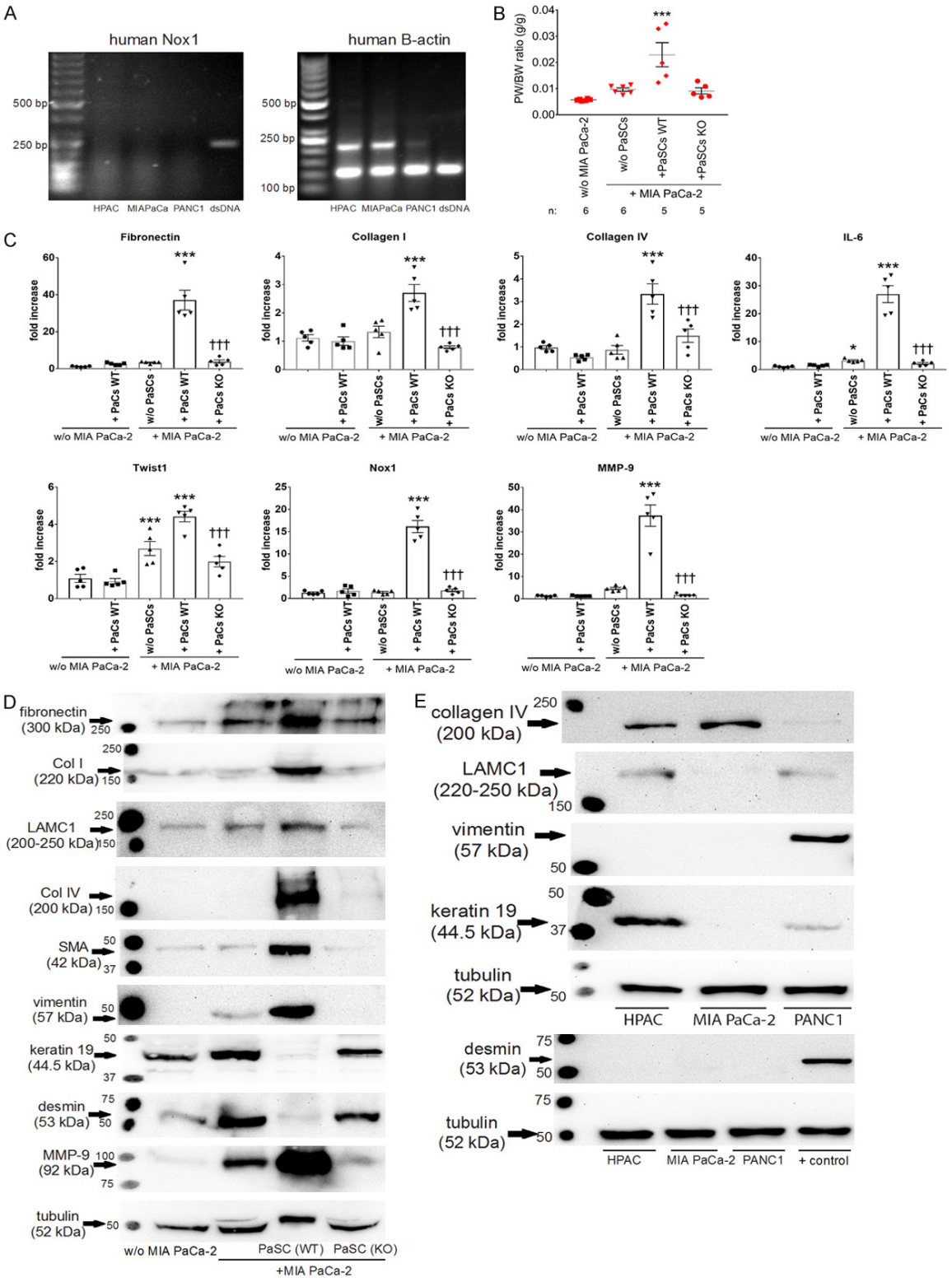

Figure 4. A. Nox1 is not expressed in pancreatic cancer cell lines HPAC, MIA Paca-2 and PANC1. We isolated total RNA from pancreatic cancer cell lines using RNeasy® Mini kit, synthesized first-strand complementary DNA with TaqMan RT-PCR kit, used one μg of complementary DNA in each PCR reaction and conducted amplification with Taq DNA polymerase from Expand High Fidelity Enzyme Mix kit using specific primers (human Nox1: Forward: 5'-TCA TCC TCG CAA GTG TGC AGA GTC-3' and Reverse: 5'-ACT TCC ATG CTG AAG CCA CGC T-3'; human actin: forward: 5'CCCAG-CACAATGAAGATCAA3'; reverse: 5'ACATCTGCTGGAAGGTGGAC3'). PCR products yielded bands of the expected size

(human Nox1: 248 bp and human actin: 103 bp). We used human DNA mix from GeneCopoeia™ as positive controls. Results were representative of 3 independent experiments. B. The lack of Nox1 in activated PaSCs with CP reduces the tumor growth in an orthotopic nude mouse model of pancreatic cancer. The pancreas of NSG™ mice was co-injected with MIA PaCa-2 cells (6-6.5 × 10^4) and activated PaSCs from *Nox1*-competent mice or *Nox1*-null mice with CP (40-60 × 10^4). At week 6, mice were euthanized and pancreas weight/body weight (PW/BW) ratio was determined. *Statistical Analysis:* One-way ANOVA followed by Student-Newman-Keuls post hoc performed by Instat Graphpad software (La Jolla, CA). ***: P<0.001 *versus* NSG™ mice without transplantation of MIA PaCa-2 or activated PaSCs with CP. n: 5 independent male mice. C. Changes in gene expression in the whole pancreas from an orthotopic xenograft model of PDAC. Data were expressed as fold change in gene expression relative to male NSG mice (mean ± SEM). 18S rRNA was used as a reference. *Statistical Analysis:* Two-way ANOVA followed by Student-Newman-Keuls post hoc was performed by Instat Graphpad software (La Jolla, CA). *: P<0.05 and ***: P<0.001 *vs* NSG mice; ††: P<0.01, and †††: P<0.001 *vs* NSG™ mice + MIA PaCa-2 cells + activated PaSCs from WT mice with CP. n: 5 independent male mice. D. The lack of Nox1 in activated PaSCs reduces stromal expansion in an orthotopic nude mouse model of pancreatic cancer. We lysed pancreatic tissues using a lysis buffer. We separated the proteins on polyacrylamide gels and transferred them to a nitrocellulose membrane. We visualized immunocomplexes with the Super Signal West Femto substrate kit. Representative immunoblots for mouse fibronectin (300 kDa), collagen IA (220 kDa), collagen IV (200 kDa), LAMC1 (220-250 kDa), αSMA (42 kDa), vimentin (57 kDa), desmin (53 kDa), MMP-9 (92 kDa), keratin 19 (TROMAIII) (44.5 kDa) were shown. n: 3 independent male mice. E. Either keratin 19 or desmin is not present in MIA PaCa-2 cells. Cell lysates of well-differentiated HPAC cells and two undifferentiated cell lines MiaPaca-2 and PANC-1 were prepared, and Western blotting analysis was carried out. Representative immunoblots for human collagen IV (200 kDa), LAMC1 (220-250 kDa), keratin 19 (TROMAIII) (44.5 kDa) and desmin (53 kDa) were shown. Higher levels of LAMC1 and keratin 19 were found in HPAC cells, while keratin 19 and desmin were absent in MIA PaCa-2 cells. A pancreatic tissue lysate from NSG™ mice + MIA PaCa-2 cells was used as a positive control of desmin. α-tubulin (52 kDa) was used as a loading control. n: 4 independent experiments.

90-alpha (gene: *Hsp90aa1*; fold change: 3.22±0.15), and Protein disulfide-isomerase A6 (gene: *Pdia6*; fold change: 2.28±0.11) (**Table 2**). Heat shock 70 kDa protein 4 (HSPA4) abundance in activated PaSCs from *Nox1*-competent mice with CP was confirmed by qPCR (**Figure 6A**). PDI abundance in activated PaSCs from *Nox1*-competent mice with CP was validated by Western blotting (**Figure 6B**).

Nox1 in activated PaSCs from mice with CP induces the production of several proteins participating in wound healing

In addition to proteins already mentioned (**Figures 1E**, **3**, **4C** and **4D**), we found that Nox1 in activated PaSCs from mice with CP induces the production of other proteins participating in wound healing as follows:

i) Connective tissue growth factor (CTGF) (gene: *Ctgf*), also known as CCN2, which is a member of the CCN family and produced by activated PaSCs [40]. We previously found that Nox1 induces the expression of transforming growth factor (TGF)-β and MMP-9 in activated PaSCs with CP [26]. Because CTGF/CCN2 acts downstream of TGF-β [41] and up-regulates MMP-9 in rat activated PaSCs [42], it was expected that Nox1 caused an up-regulation of CTGF/CCN2 in activated PaSCs from mice with CP (fold change: 4.83±0.41) (**Table 2**). This finding was confirmed by qPCR (**Figure 6A**) and Western blotting (**Figure 6B**).

ii) Protein-glutamine gamma-glutamyltransferase 2 (TGM2) (Gene: *Tgm2*) is a calcium-dependent acyltransferase that catalyzes the formation of covalent bonds between peptide-bound glutamine and various primary amines, thereby producing cross-linked or aminated proteins in the extracellular compartment [43]. Based on the mass spectrometry, Nox1 induced the expression of TGM2 in activated PaSCs from mice with CP (fold change: 4.70±0.19) (**Table 2**). This finding was confirmed by qPCR (**Figure 6A**).

iii) Insulin-like growth factor-binding protein 2 (IGFBP2) (gene: *Igfbp2*). IGF can bind to both their receptors, IGFRs, and IGFBPs. When IGFs bind to IGFBPs, IGFBPs prolong the half-life of IGFs, and facilitate their distribution to target tissues. However, when IGFBPs are up-regulated, IGFBPs inhibit the interaction of IGFs with their receptors, and consequently, the intracellular IGF signaling [44]. There are seven distinct types of IGFBPs (IGFBP1 through IGFBP7). Based on the mass spectrometry, we found IGFBP2, IGFBP6 and IGFBP7 in the CM of activated PaSCs from *Nox1*-competent mice with CP. In particular, Nox1 induced the production of IGFBP2 in activated PaSCs from mice with CP (4.22±0.39) (**Table 2**). This finding was confirmed by qPCR (**Figure 6A**).

Other proteins involving in wound healing and regulating by Nox1 are listed in **Table 2**. The level of periostin slightly increased in activated

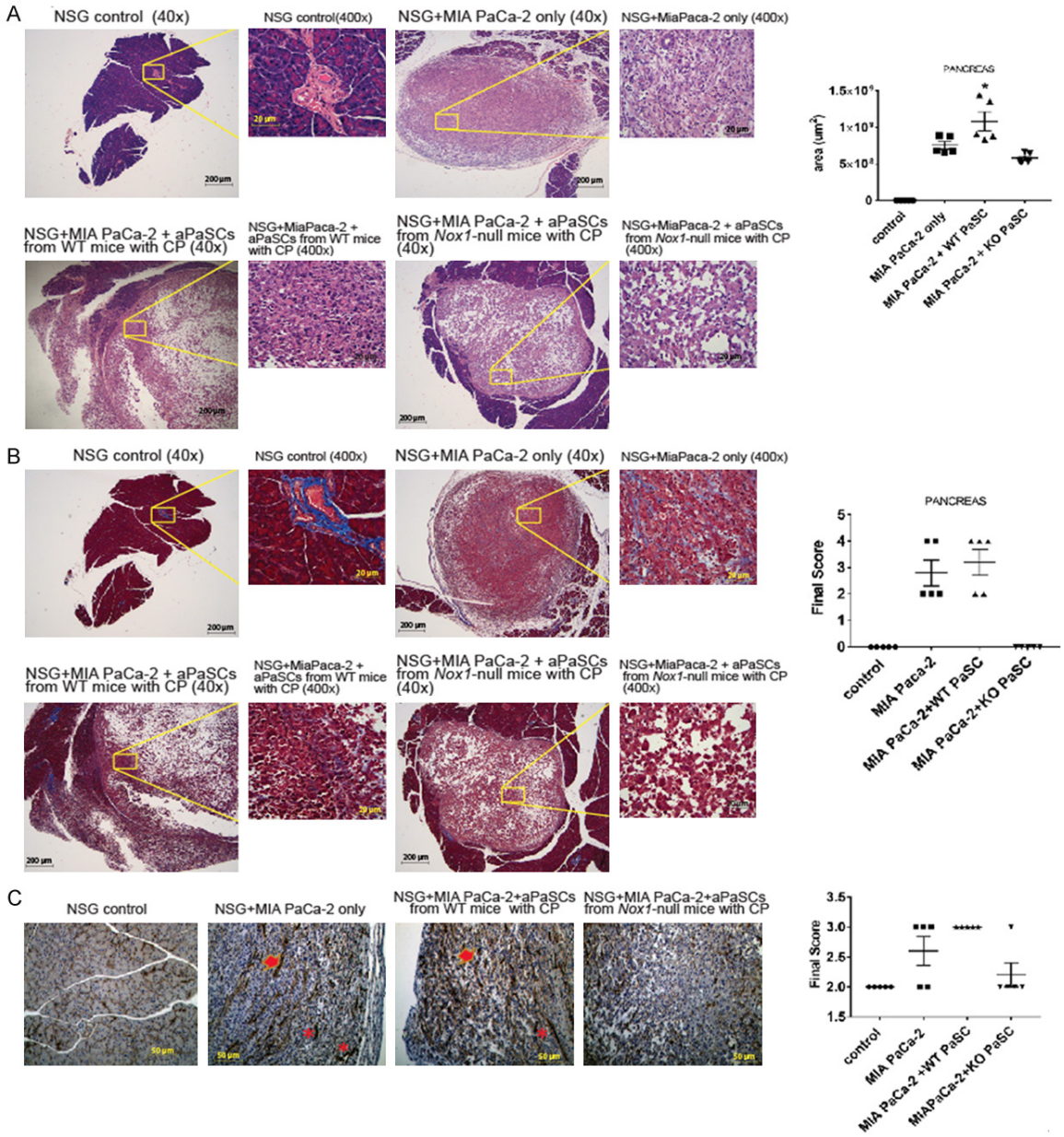

Figure 5. A. H&E staining: Representative H&E stained sections showed that the invasive malignant focuses in all of these tissues were poorly differentiated, had a very prominent rhabdoid morphology. The tumor in the pancreas co-injected with MIA PaCa-2 cells and activated PaSCs (aPaSCs) from *Nox1*-compentent mice with CP had the most infiltrative appearance at the borders, while the others had more circumscribed borders. Quantitative analysis showed the area (um^2) of the invasive malignant focuses. *Statistical Analysis:* One-way ANOVA followed by Student-Newman-Keuls post hoc performed by Instat Graphpad software (La Jolla, CA). *: P<0.05 vs male NSG^{TM} mice + MIA PaCa-2 cells. n: 5 independent mice. B. Masson's Trichrome staining: pancreas: Representative Masson's Trichrome stained sections show that the invasive malignant focuses did not display abundant desmoplastic stroma. Total magnification: 40 × (left) and 400 × (right). n: 5 independent mice. Quantitative analysis showed the final score. C. Mouse fibroblasts are the sources of Collagen IV in the orthotopic xenograft model of PDAC. Pancreatic tissues were fixed with 10% formalin and embedded in paraffin. Following incubation with antibody against mouse collagen IV, positive cells were visualized using 3,3'-diaminobenzidine tetrahydrochloride (DAB) as a chromogen (color: brown). Red arrow: collagen IV-positive fibroblasts; red asterisk: Collagen IV in basement membrane (perivascular staining). Total magnification: 200 ×. n: 5 independent mice. Quantitative analysis showed the final score.

PaSCs from *Nox1*-competent mice with CP (**Figure 6B**). However, the lack of Nox1 did not affect its production by activated PaSCs (fold change: 0.69±0.03) (ProteomeXchange with identifier PXD034177). This finding was confirmed by Western blotting (**Figure 6B**).

Table 2. Comparative abundance of secreted proteins in CM of activated PaSCs from Nox1-competent and Nox1-null mice with CP

Protein	Fold increase
chaperones protecting from endoplasmic reticulum stress	
Heat shock 70 kDa protein 4 OS=*Mus musculus* GN=Hspa4 PE=1 SV=1 - [HSP74_MOUSE]	12.13±0.99
Heat shock cognate 71 kDa protein OS=*Mus musculus* GN=Hspa8 PE=1 SV=1 - [HSP7C_MOUSE]	4.02±0.41
Heat shock protein HSP 90-alpha OS=*Mus musculus* GN=Hsp90aa1 PE=1 SV=4 - [HS90A_MOUSE]	3.22±0.15
Protein disulfide-isomerase A6 OS=*Mus musculus* GN=Pdia6 PE=1 SV=3 - [PDIA6_MOUSE]	2.28±0.11
Proteins participating in wound healing	
Connective tissue growth factor OS=*Mus musculus* GN=Ctgf PE=2 SV=3 - [CTGF_MOUSE]	4.83±0.41
Protein-glutamine gamma-glutamyltransferase 2 OS=*Mus musculus* GN=Tgm2 PE=1 SV=4 - [TGM2_MOUSE]	4.70±0.19
Insulin-like growth factor-binding protein 2 OS=*Mus musculus* GN=Igfbp2 PE=2 SV=2 - [IBP2_MOUSE]	4.22±0.39
Proteins protecting against oxidative stress	
Peroxiredoxin-4 OS=*Mus musculus* GN=Prdx4 PE=1 SV=1 - [PRDX4_MOUSE]	6.57±0.57
Thioredoxin reductase 1, cytoplasmic OS=*Mus musculus* GN=Txnrd1 PE=1 SV=3 - [TRXR1_MOUSE]	4.14±0.20
Peroxiredoxin-1 OS=*Mus musculus* GN=Prdx1 PE=1 SV=1 - [PRDX1_MOUSE]	3.75±0.22
Proteins protecting from metabolic stress	
Pyruvate kinase PKM OS=*Mus musculus* GN=Pkm PE=1 SV=4 - [KPYM_MOUSE]	3.95±0.12

The table provides protein names, and the fold increase, which is the *Nox1*-competent mice to *Nox1*-null mice predominant ratios of the averaged PSMs and standard error of the mean (SEM) for specific proteins using normalized spectral counts. We focused on proteins that were at least 2.5-fold more abundant in CM of PaSCs from *Nox1*-competent mice with CP (cut off: 2.5-fold change) and their SEM were lower than 10% of fold change (mean). Overall, a total of 104 proteins were identified in the CM across the ten samples (5 CM of PaSCs from *Nox1*-competent mice with CP, 5 CM of PaSCs from *Nox1*-null mice with CP) and analyzed.

Nox1 in activated PaSCs from mice with CP induces the production of proteins protecting cancer cells against oxidative stress

The cytosolic (secreted) selenoprotein flavin adenine dinucleotide oxidoreductase thioredoxin reductase 1 (TrxR1) (gene: *Txnrd1*) supports several processes crucial for cell function, cell proliferation, antioxidant defense and redox-regulated signaling cascades [45]. Nox1 induced the production of TrxR1 in activated PaSCs from mice with CP (fold change: 4.14± 0.20) (**Table 2**). This finding was confirmed by qPCR (**Figure 6A**) and Western blotting (**Figure 6B**). The antioxidant enzymes that are either directly or indirectly supported by TrxR1 include peroxiredoxins (Prdxs) and thioredoxin 1 (Trx1), among others [46].

i) Prdxs are abundant thiol-dependent peroxidases [46]. Four Prdxs are cytosolic (Prdx1, Prdx2, Prdx4, and Prdx6) and two are mitochondrial (Prdx3 and Prdx5). Those cytosolic Prdxs can be secreted, possibly via a non-classical secretory pathway [47]. Using RT-PCR, Prdxs 1, 2, 4 and 6 were found in pancreas from heathy mice and mice with CP (**Figure 6C**). Based on the mass spectrometry, the most affected cytosolic isoforms by Nox1-induced cytosolic TrxR1 were Prdx4 (fold change: 6.58±0.57) and Prdx1 (fold change: 3.75±0.22) (**Table 2**). These findings were confirmed by qPCR (**Figure 6A**) and Western blotting (**Figure 6B**).

ii) Trx1 (gene: Txn) is a cytosolic 12-kDa protein with a broad capacity of catalyzing disulfide reduction in many substrate proteins [48]. Although we found Trx1 in the secretome of activated PaSCs from both *Nox1*-competent and *Nox1*-null mice with CP, its content was similar in both secretomes (fold change: 0.93±0.09) (ProteomeXchange with identifier PXD034177).

Nox1 in activated PaSCs from mice with CP induced the production of proteins protecting cancer cells from metabolic stress

Glycolysis facilitates routing the carbon skeletons into the oxidative pentose phosphate pathway (also called the phosphogluconate pathway and the hexose monophosphate shunt), which is a metabolic pathway parallel to glycolysis that generates NADPH and pentoses [49]. Nox1 uses NADPH to generate ROS, which is essential for the fibrogenic activity of activated PaSCs from mice with CP. Here, we found that Nox1 stimulated glycolysis by producing

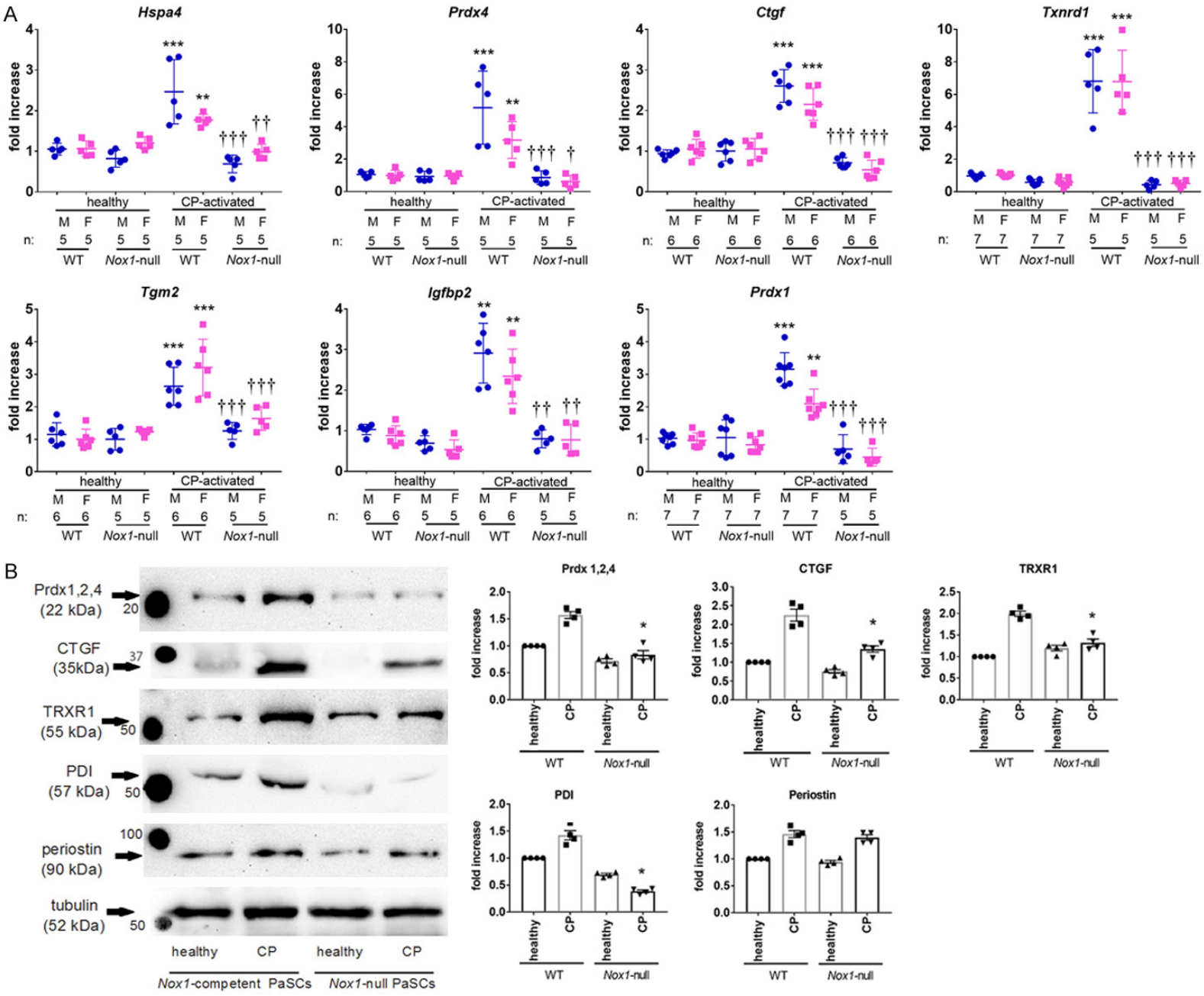
A
Hspa4
Prdx4
Ctgf
Txnrd1
Tgm2
Igfbp2
Prdx1
fold increase
healthy
CP-activated
M F M F M F M F
WT
Nox1-null
B
Prdx1,2,4 (22 kDa)
CTGF (35kDa)
TRXR1 (55 kDa)
PDI (57 kDa)
periostin (90 kDa)
tubulin (52 kDa)
healthy
CP
Nox1-competent PaSCs
Nox1-null PaSCs
Prdx 1,2,4
CTGF
TRXR1
PDI
Periostin

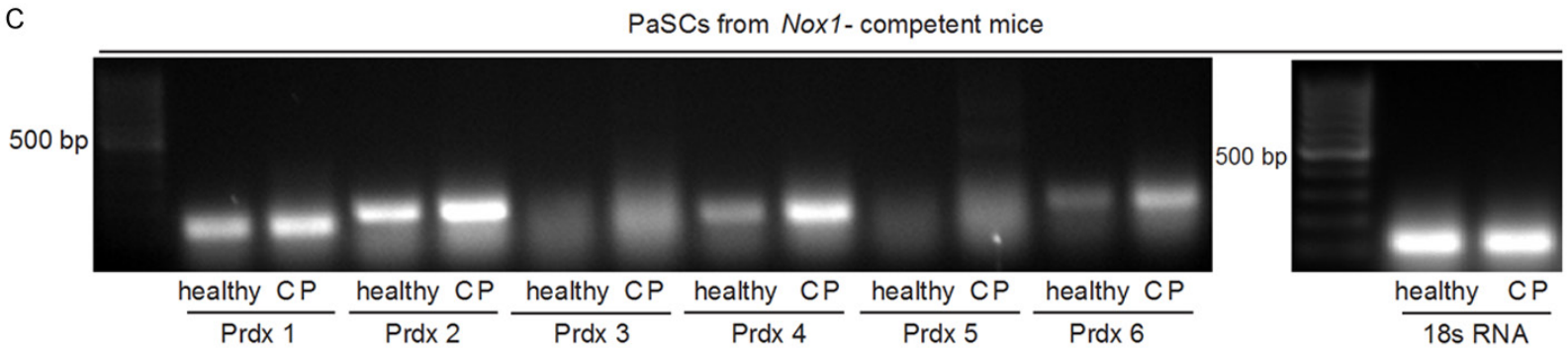

Figure 6. Nox1 in activated PaSCs from mice with CP induces the production of several proteins protecting from ER, oxidative and metabolic stresses. A. Validation of mass spectrometry using quantitative PCR. Data were expressed as fold change in gene expression relative to activated PaSCs from *Nox1*-competent healthy mice (male or female) (mean ± SEM). 18S rRNA was used as a reference. *Statistical Analysis:* One-way ANOVA followed by Student-Newman-Keuls post hoc was performed by Instat Graphpad software (La Jolla, CA). *: P<0.05, **: P<0.01, and ***: P<0.001 *vs* WT mice; ††: P<0.01, and †††: P<0.001 *vs* WT mice with CP. n: as indicated in the figure. B. Nox1 in activated PaSCs from mice with CP induces the production of Prdx1, Prdx4, CTGF, TRXR1 and PDI. We lysed activated PaSCs from *Nox1*-competent and *Nox1*-null mice with or without CP and carried out Western blotting analysis. Left: Representative immunoblots for Prdxs 1, 2, 4 (22 kDa), CTGF (35 kDa), TRXR1 (55 kDa), PDI (57 kDa) and periostin (90 kDa) were shown. α-tubulin (52 kDa) was used as a loading control. n: 4. Right: The quantitative analysis was performed using density analysis software from TotalLab Quant TL100 (Newcastle upon Tyne, UK). *Statistical Analysis:* One-way ANOVA followed by Student-Newman-Keuls post hoc was performed by Instat Graphpad software (La Jolla, CA). *: P<0.05 *vs* WT mice with CP. n: 4 independent experiments. C. Prdxs 1, 2, 4, and 6 isoforms are expressed in pancreatic tissues. We isolated total RNA from pancreatic tissues of healthy mice and mice with CP using Trizol and RNeasy® Mini kit, synthesized first-strand complementary DNA with TaqMan RT-PCR kit, used four μg of complementary DNA in each PCR reaction and conducted amplification with Taq DNA polymerase from Expand High Fidelity Enzyme Mix kit using specific primers (**Table 1**). n: Results were representative of 3 independent experiments.

pyruvate kinase (gene: Pkm; fold change: 3.95±0.12) (**Table 2**), which catalyzes the transfer of a phosphate group from phosphoenolpyruvate to ADP, generating ATP (a substrate level-phosphorylation).

Discussion

First, we compared the ability of Nox1 in activated PaSCs from mice with or without CP to facilitate the invasion/migration of pancreatic cancer cells. *In vitro,* using a cell invasion assay and a scratch wound migration assay, activated PaSCs from mice with CP display a more pro-invasive/migratory phenotype than activated PaSCs from healthy mice in a Nox1 signaling-dependent manner. Unlike activated PaSCs from mice with CP, the presence of activated PaSCs from healthy mice did not cause a significant increase in cancer cell migration/invasion.

Regarding the mechanism by which Nox1 increased cancer cell migration/invasion, we previously found that Nox1 increased the expression of MMP-9 and Twist1 in activated PaSCs from mice with CP [26]. Twist1 is a transcription factor within the basic helix-loop-helix (bHLH) family present in high amounts in human bone marrow-derived mesenchymal stromal and stem cells [50]. Twist1 has directly induced the expression of MMP-9 in astrocytoma [51] and in human peritoneal mesothelial cells [52]. MMP-9 is a gelatinase that degrades ECM proteins, including elastins, fibronectin, and collagens (e.g., collagen IV in the basal lamina) [16]. Because activated PaSCs from mice with CP expressed MMP-9 and Twist1 at much higher levels than activated PaSCs from healthy mice (untreated with caerulein) [26], and MMP-9 and Twist1 mRNA levels were enhanced by the presence of pancreatic cancer cell lines and reduced by the lack of Nox1, we concluded that the Twist1/MMP-9 signaling represents a mechanism by which Nox1 in activated PaSCs facilitates the migration/invasion of cancer cells in a mouse model of CP.

Because the scratch wound assay was carried out for more than 24 h, the wound closure could be caused by a combination of both cell proliferation and migration. Because, Nox1 has not affected the proliferation of colon cancer cell lines [53], while it has facilitated the invasion of Kras-transformed rat kidney fibroblast cells through MMP-9 [28], the wound closure was mainly caused by a pro-migratory phenotype of activated PaSCs from mice with CP.

In healthy pancreas, activated PaSCs maintain the balance between the synthesis and degradation of the basal lamina [54], mainly composed of collagen IV and LAMC1 [55], whereas in CP, activated PaSCs form the stroma [14], mainly composed of collagen I and fibronectin [55]. *In vitro,* we found that the induction of CP increased the expression of fibronectin, and to a lesser extent, collagen I in activated PaSCs, and that both LAMC1 and Collagen IV were still being produced by activated PaSCs even during CP-induced healing process. We also discovered that Nox1 participates in the formation of the stroma because the deletion of *Nox1* reduced the expression of fibronectin, LAMC1, collagen I, and collagen IV in activated PaSCs from mice with CP. Therefore, we can conclude that secreted proteins were produced by activated PaSCs from mice with CP following Nox1 activation to cause ECM dynamic changes (e.g., fibronectin, collagens, LAMC1, MMP-9) and stimulate migration/invasion of pancreatic cancer cells.

There are at least two main types of PaSCs/CAFs: tumor-promoting (high level of IL-6; low level of αSMA) and tumor-restraining (low level of IL-6; high level of αSMA) [56]. We found that activated PaSCs from mice with CP are tumor-promoting because these PaSCs facilitated the invasion/migration of pancreatic cancer cells via Nox1. To confirm this assumption, we compared the expression of αSMA and IL-6 in activated PaSCs from mice with or without CP expressing or not Nox1. We found that the induction of CP in mice increases the level of αSMA in activated PaSCs in a Nox1-independent manner, without affecting the expression of IL-6. For that, the classification of SMA + PaSCs as tumor-restraining needs to be further discussed.

In vivo, using an orthotopic xenograft model of PDAC, we found that Nox1 in activated PaSCs from mice with CP facilitated the growth of MIA PaCa-2 cells and the expansion of stromal compartment, as evaluated by staining with Masson's trichrome and representative immunoblots for αSMA, vimentin, fibronectin and collagen 1A. We found that the expanded population of PaSCs/CAFs in the presence of MIA

PaCa-2 cells secrete more fibronectin than collagen I because collagen I at both mRNA and protein levels was lower than fibronectin in the pancreas from NSG™ mice co-injected with MIA PaCa-2 and activated PaSCs from *Nox1*-competent mice with CP. We also discovered that the expanded population of PaSCs/CAFs in the presence of MIA PaCa-2 cells was desmin-negative and αSMA-positive, as evaluated by representative immunoblots for desmin and αSMA, and this population required Nox1 to be expanded.

In vivo, Nox1 in activated PaSCs from mice with CP was required for an ECM dynamic change since the co-injection of activated PaSCs from *Nox1*-competent mice with CP with MIA PaCa-2 cells in the pancreas of immunodeficient NSG™ mice increased MMP-9 at mRNA and protein levels, whereas the co-injection of activated PaSCs from male *Nox1*-null mice with CP and MIA PaCa-2 cells diminished MMP-9 at mRNA and protein levels. There are two main sources of MMP-9 in PDAC/CP: activated PaSCs and macrophages [57]. We previously found that Nox1 in activated PaSCs from mice with CP evoked a higher expression of MMP-9 than in those cells from healthy mice [26]. Because NSG™ mice have defective macrophages [33], it was likely that MMP-9 comes from activated PaSCs/CAFs, rather than macrophages.

Therefore, we can also conclude that when activated PaSCs from mice with CP were co-injected with MIA PaCa-2 cells in the pancreas of NSG™ mice, activated PaSCs/CAFs, which were desmin-negative and αSMA-positive, facilitated the growth of pancreatic cancer cells by causing MMP9-dependent ECM dynamic changes. However, because Nox1 is expressed in endothelial cells [58], pericytes [59] and smooth muscle cells [32], which are cells other than PaSCs present in the stroma, we cannot rule out the participation of other sources of Nox1 as influencers of tumor progression.

Next, we explored the mechanisms by which Nox1 in activated PaSCs from mice with CP paracrinally facilitates cancer progression by identifying Nox1-evoked secreted proteins using mass spectrometry. We showed that Nox1 in activated PaSCs from mice with CP protects cancer cells from ER stress by producing HSPA4 and PDI6. These findings were supported by the fact that in vascular smooth muscle cells Nox1 has regulated ER homeostasis by colocalizing with PDI [60].

Based on the mass spectrometry, Nox1 in activated PaSCs from mice with CP also protected cancer cells against oxidative stress by producing TrxR1, Prdx4, and to a lesser extent, Prdx1. TrxR1 supports several processes crucial for cell function, cell proliferation, antioxidant defense and redox-regulated signaling cascades [45]. Prdxs are antioxidant enzymes that are either directly or indirectly supported by TrxR1 [46]. Using RT-PCR, Prdxs 1, 2, 4 and 6 were found in pancreas from heathy mice and mice with CP. However, the most affected cytosolic isoforms by Nox1-induced cytosolic TrxR1 were Prdx4 and Prdx1. Based on these findings, we believe that both Prdxs were overexpressed and secreted as a mechanism to eliminate the excess Nox1-derived ROS in activated PaSCs from mice with CP.

Nox1 in activated PaSCs from mice with CP also participated in wound healing since Nox1 induced the production of CTGF, TGM2, and IGFBP2, and protected cancer cells from metabolic stress because Nox1 induced the expression of pyruvate kinase.

In conclusion, Nox1 in activated PaSCs from mice with CP facilitates the progression of PDAC not only by inducing the expression of MMP-9, but also the production of proteins protecting from ER, oxidative and metabolic stresses. Therefore, inhibiting Nox1 signaling in activated PaSCs from patients with CP at early stages can reduce both the ECM dynamic changes and the production of proteins protecting from ER, oxidative and metabolic stresses, ameliorating the progression of PDAC.

Acknowledgements

We thank Donna Kumiski from the Histology core of Augusta University for her excellent work. This work was supported by the Augusta University Provost's office, the Translational Research Program of the Department of Medicine, Medical College of Georgia, the Scholarship & Creative Activity (RSCA), and the National Institutes of Health National Cancer Institute grant (1R15CA267836-01A1) awarded to M.E.S.

Disclosure of conflict of interest

None.

Abbreviations

ANOVA, analysis of variance; aPaSCs, activated PaSCs; BSA, bovine albumin serum; BSL-2, Biosafety Level 2; CAFs, cancer-associated fibroblasts; cDNA, complementary deoxyribonucleic acid; CM, conditioned media; CP, chronic pancreatitis; CTGF, connective tissue growth factor; DAB, 3,3-diaminobenzidine tetrahydrochloride; DMEM, Dulbecco's minimal essential medium; dsDNA, double strand DNA; ECM, extracellular matrix; ER, endoplasmic reticulum; F, female; FBS, fetal bovine serum; H&E, Hematoxylin and eosin; HRP, horseradish peroxidase; HSPA4, Heat shock 70 kDa protein 4; IACUC, Institutional Animal Care and Use Committee; IDV, integrated density volume; IGF, Insulin-like growth factor; IGFBP2, Insulin-like growth factor-binding protein 2; IHC, immunohistochemistry; IL-6, interleukin-6; IMDM, Iscove's Modified Dulbecco's medium; KO, knock out; LAMC1, laminin gamma-1; LC-MS/MS, liquid chromatography with tandem mass spectrometry; M, male; MGI, Mouse Genome Informatics; MMPs, matrix metalloproteinases; mRNA, messenger ribonucleic acid; Nox1, NADPH oxidase 1; PanIN, pancreatic intraepithelial neoplasia; PaSCs, Pancreatic stellate cells; PDAC, pancreatic ductal adenocarcinoma; PDI, Protein disulfide-isomerase; Prdx, peroxiredoxin; PSM, peptide spectrum matching; PW/BW ratio, pancreas weight/body weight ratio; qPCR, quantitative polymerase chain reaction; ROS, reactive oxygen species; RT-PCR, reverse transcriptase-polymerase chain reaction; SDS, sodium dodecyl sulfate; SEM, standard error of mean; αSMA, α-smooth muscle actin; SOD, superoxide dismutase; TBST, Tris-buffered saline containing 0.1% (v/v) Tween X-20; TGF-β, transforming growth factor-β; TGM2, Protein-glutamine gamma-glutamyltransferase 2; Trx1, thioredoxin 1; TrxR1, thioredoxin reductase 1; w/, with; w/o, without; WT, wild type (it is also called *Nox1*-competent).

Address correspondence to: Dr. Maria E Sabbatini, Department of Biological Sciences, Augusta University, C2014 Science Hall, 2500 Walton Way, Augusta, Georgia 30904, USA. E-mail: msabbatini@augusta.edu

References

[1] Yadav D and Lowenfels AB. The epidemiology of pancreatitis and pancreatic cancer. Gastroenterology 2013; 144: 1252-1261.

[2] Apte MV, Haber PS, Applegate TL, Norton ID, McCaughan GW, Korsten MA, Pirola RC and Wilson JS. Periacinar stellate shaped cells in rat pancreas: identification, isolation, and culture. Gut 1998; 43: 128-133.

[3] Andea A, Sarkar F and Adsay VN. Clinicopathological correlates of pancreatic intraepithelial neoplasia: a comparative analysis of 82 cases with and 152 cases without pancreatic ductal adenocarcinoma. Mod Pathol 2003; 16: 996-1006.

[4] Guerra C, Schuhmacher AJ, Canamero M, Grippo PJ, Verdaguer L, Perez-Gallego L, Dubus P, Sandgren EP and Barbacid M. Chronic pancreatitis is essential for induction of pancreatic ductal adenocarcinoma by K-Ras oncogenes in adult mice. Cancer Cell 2007; 11: 291-302.

[5] Basturk O, Hong SM, Wood LD, Adsay NV, Albores-Saavedra J, Biankin AV, Brosens LA, Fukushima N, Goggins M, Hruban RH, Kato Y, Klimstra DS, Kloppel G, Krasinskas A, Longnecker DS, Matthaei H, Offerhaus GJ, Shimizu M, Takaori K, Terris B, Yachida S, Esposito I and Furukawa T; Baltimore Consensus Meeting. A revised classification system and recommendations from the baltimore consensus meeting for neoplastic precursor lesions in the pancreas. Am J Surg Pathol 2015; 39: 1730-1741.

[6] Malka D, Hammel P, Maire F, Rufat P, Madeira I, Pessione F, Levy P and Ruszniewski P. Risk of pancreatic adenocarcinoma in chronic pancreatitis. Gut 2002; 51: 849-852.

[7] Hwang RF, Moore T, Arumugam T, Ramachandran V, Amos KD, Rivera A, Ji B, Evans DB and Logsdon CD. Cancer-associated stromal fibroblasts promote pancreatic tumor progression. Cancer Res 2008; 68: 918-926.

[8] Bachem MG, Schunemann M, Ramadani M, Siech M, Beger H, Buck A, Zhou S, Schmid-Kotsas A and Adler G. Pancreatic carcinoma cells induce fibrosis by stimulating proliferation and matrix synthesis of stellate cells. Gastroenterology 2005; 128: 907-921.

[9] Whittle MC and Hingorani SR. Fibroblasts in pancreatic ductal adenocarcinoma: biological mechanisms and therapeutic targets. Gastroenterology 2019; 156: 2085-2096.

[10] Pothula SP, Xu Z, Goldstein D, Pirola RC, Wilson JS and Apte MV. Key role of pancreatic stellate cells in pancreatic cancer. Cancer Lett 2016; 381: 194-200.

[11] Lo A, Wang LS, Scholler J, Monslow J, Avery D, Newick K, O'Brien S, Evans RA, Bajor DJ, Clen-

denin C, Durham AC, Buza EL, Vonderheide RH, June CH, Albelda SM and Pure E. Tumor-promoting desmoplasia is disrupted by depleting FAP-expressing stromal cells. Cancer Res 2015; 75: 2800-2810.
[12] Olive KP, Jacobetz MA, Davidson CJ, Gopinathan A, McIntyre D, Honess D, Madhu B, Goldgraben MA, Caldwell ME, Allard D, Frese KK, Denicola G, Feig C, Combs C, Winter SP, Ireland-Zecchini H, Reichelt S, Howat WJ, Chang A, Dhara M, Wang L, Ruckert F, Grutzmann R, Pilarsky C, Izeradjene K, Hingorani SR, Huang P, Davies SE, Plunkett W, Egorin M, Hruban RH, Whitebread N, McGovern K, Adams J, Iacobuzio-Donahue C, Griffiths J and Tuveson DA. Inhibition of Hedgehog signaling enhances delivery of chemotherapy in a mouse model of pancreatic cancer. Science 2009; 324: 1457-1461.
[13] Tomasek JJ, Gabbiani G, Hinz B, Chaponnier C and Brown RA. Myofibroblasts and mechano-regulation of connective tissue remodelling. Nat Rev Mol Cell Biol 2002; 3: 349-363.
[14] Apte MV, Wilson JS, Lugea A and Pandol SJ. A starring role for stellate cells in the pancreatic cancer microenvironment. Gastroenterology 2013; 144: 1210-1219.
[15] Habtezion A, Edderkaoui M and Pandol SJ. Macrophages and pancreatic ductal adenocarcinoma. Cancer Lett 2016; 381: 211-216.
[16] Coussens LM, Fingleton B and Matrisian LM. Matrix metalloproteinase inhibitors and cancer: trials and tribulations. Science 2002; 295: 2387-2392.
[17] Kleeff J, Whitcomb DC, Shimosegawa T, Esposito I, Lerch MM, Gress T, Mayerle J, Drewes AM, Rebours V, Akisik F, Munoz JED and Neoptolemos JP. Chronic pancreatitis. Nat Rev Dis Primers 2017; 3: 17060.
[18] Bedard K and Krause KH. The NOX family of ROS-generating NADPH oxidases: physiology and pathophysiology. Physiol Rev 2007; 87: 245-313.
[19] Laurent E, McCoy JW 3rd, Macina RA, Liu W, Cheng G, Robine S, Papkoff J and Lambeth JD. Nox1 is over-expressed in human colon cancers and correlates with activating mutations in K-Ras. Int J Cancer 2008; 123: 100-107.
[20] Lim SD, Sun C, Lambeth JD, Marshall F, Amin M, Chung L, Petros JA and Arnold RS. Increased Nox1 and hydrogen peroxide in prostate cancer. Prostate 2005; 62: 200-207.
[21] Chamulitrat W, Schmidt R, Tomakidi P, Stremmel W, Chunglok W, Kawahara T and Rokutan K. Association of gp91phox homolog Nox1 with anchorage-independent growth and MAP kinase-activation of transformed human keratinocytes. Oncogene 2003; 22: 6045-6053.
[22] Suh YA, Arnold RS, Lassegue B, Shi J, Xu X, Sorescu D, Chung AB, Griendling KK and Lambeth JD. Cell transformation by the superoxide-generating oxidase Mox1. Nature 1999; 401: 79-82.
[23] Mitsushita J, Lambeth JD and Kamata T. The superoxide-generating oxidase Nox1 is functionally required for Ras oncogene transformation. Cancer Res 2004; 64: 3580-3585.
[24] Asaumi H, Watanabe S, Taguchi M, Tashiro M and Otsuki M. Externally applied pressure activates pancreatic stellate cells through the generation of intracellular reactive oxygen species. Am J Physiol Gastrointest Liver Physiol 2007; 293: G972-G978.
[25] Masamune A, Watanabe T, Kikuta K, Satoh K and Shimosegawa T. NADPH oxidase plays a crucial role in the activation of pancreatic stellate cells. Am J Physiol Gastrointest Liver Physiol 2008; 294: G99-G108.
[26] Xia D, Halder B, Godoy C, Chakraborty A, Singla B, Thomas E, Shuja JB, Kashif H, Miller L, Csanyi G and Sabbatini ME. NADPH oxidase 1 mediates caerulein-induced pancreatic fibrosis in chronic pancreatitis. Free Radic Biol Med 2020; 147: 139-149.
[27] Hu R, Wang YL, Edderkaoui M, Lugea A, Apte MV and Pandol SJ. Ethanol augments PDGF-induced NADPH oxidase activity and proliferation in rat pancreatic stellate cells. Pancreatology 2007; 7: 332-340.
[28] Shinohara M, Adachi Y, Mitsushita J, Kuwabara M, Nagasawa A, Harada S, Furuta S, Zhang Y, Seheli K, Miyazaki H and Kamata T. Reactive oxygen generated by NADPH oxidase 1 (Nox1) contributes to cell invasion by regulating matrix metalloprotease-9 production and cell migration. J Biol Chem 2010; 285: 4481-4488.
[29] Miller C, Cai Y, Patton T, Graves SH, Li H and Sabbatini ME. RCAD/BiP pathway is necessary for the proper synthesis of digestive enzymes and secretory function of the exocrine pancreas. Am J Physiol Gastrointest Liver Physiol 2017; 312: G314-G326.
[30] Quinn SN, Graves SH, Dains-McGahee C, Friedman EM, Hassan H, Witkowski P and Sabbatini ME. Adenylyl cyclase 3/adenylyl cyclase-associated protein 1 (CAP1) complex mediates the anti-migratory effect of forskolin in pancreatic cancer cells. Mol Carcinog 2017; 56: 1344-1360.
[31] Deer EL, Gonzalez-Hernandez J, Coursen JD, Shea JE, Ngatia J, Scaife CL, Firpo MA and Mulvihill SJ. Phenotype and genotype of pancreatic cancer cell lines. Pancreas 2010; 39: 425-435.
[32] Gavazzi G, Banfi B, Deffert C, Fiette L, Schappi M, Herrmann F and Krause KH. Decreased blood pressure in NOX1-deficient mice. FEBS Lett 2006; 580: 497-504.
[33] Shultz LD, Lyons BL, Burzenski LM, Gott B, Chen X, Chaleff S, Kotb M, Gillies SD, King M,

Mangada J, Greiner DL and Handgretinger R. Human lymphoid and myeloid cell development in NOD/LtSz-scid IL2R gamma null mice engrafted with mobilized human hemopoietic stem cells. J Immunol 2005; 174: 6477-6489.
[34] Neuschwander-Tetri BA, Burton FR, Presti ME, Britton RS, Janney CG, Garvin PR, Brunt EM, Galvin NJ and Poulos JE. Repetitive self-limited acute pancreatitis induces pancreatic fibrogenesis in the mouse. Dig Dis Sci 2000; 45: 665-674.
[35] Pijuan J, Barcelo C, Moreno DF, Maiques O, Siso P, Marti RM, Macia A and Panosa A. In vitro cell migration, invasion, and adhesion assays: from cell imaging to data analysis. Front Cell Dev Biol 2019; 7: 107.
[36] Livak KJ and Schmittgen TD. Analysis of relative gene expression data using real-time quantitative PCR and the 2(-Delta Delta C(T)) method. Methods 2001; 25: 402-408.
[37] Sans MD, Sabbatini ME, Ernst SA, D'Alecy LG, Nishijima I and Williams JA. Secretin is not necessary for exocrine pancreatic development and growth in mice. Am J Physiol Gastrointest Liver Physiol 2011; 301: G791-G798.
[38] Ideno N, Yamaguchi H, Ghosh B, Gupta S, Okumura T, Steffen DJ, Fisher CG, Wood LD, Singhi AD, Nakamura M, Gutkind JS and Maitra A. GNAS(R201C) induces pancreatic cystic neoplasms in mice that express activated KRAS by inhibiting YAP1 signaling. Gastroenterology 2018; 155: 1593-1607, e1512.
[39] Deutsch EW, Csordas A, Sun Z, Jarnuczak A, Perez-Riverol Y, Ternent T, Campbell DS, Bernal-Llinares M, Okuda S, Kawano S, Moritz RL, Carver JJ, Wang M, Ishihama Y, Bandeira N, Hermjakob H and Vizcaino JA. The ProteomeXchange consortium in 2017: supporting the cultural change in proteomics public data deposition. Nucleic Acids Res 2017; 45: D1100-D1106.
[40] Gao R and Brigstock DR. Connective tissue growth factor (CCN2) in rat pancreatic stellate cell function: integrin alpha5beta1 as a novel CCN2 receptor. Gastroenterology 2005; 129: 1019-1030.
[41] Holmes A, Abraham DJ, Sa S, Shiwen X, Black CM and Leask A. CTGF and SMADs, maintenance of scleroderma phenotype is independent of SMAD signaling. J Biol Chem 2001; 276: 10594-10601.
[42] Karger A, Fitzner B, Brock P, Sparmann G, Emmrich J, Liebe S and Jaster R. Molecular insights into connective tissue growth factor action in rat pancreatic stellate cells. Cell Signal 2008; 20: 1865-1872.
[43] Griffin M, Casadio R and Bergamini CM. Transglutaminases: nature's biological glues. Biochem J 2002; 368: 377-396.
[44] Thomas D and Radhakrishnan P. Role of tumor and stroma-derived IGF/IGFBPs in pancreatic cancer. Cancers (Basel) 2020; 12: 1228.
[45] Soderberg A, Sahaf B and Rosen A. Thioredoxin reductase, a redox-active selenoprotein, is secreted by normal and neoplastic cells: presence in human plasma. Cancer Res 2000; 60: 2281-2289.
[46] Arner ES. Focus on mammalian thioredoxin reductases--important selenoproteins with versatile functions. Biochim Biophys Acta 2009; 1790: 495-526.
[47] Nicolussi A, D'Inzeo S, Capalbo C, Giannini G and Coppa A. The role of peroxiredoxins in cancer. Mol Clin Oncol 2017; 6: 139-153.
[48] Ren X, Zou L, Zhang X, Branco V, Wang J, Carvalho C, Holmgren A and Lu J. Redox signaling mediated by thioredoxin and glutathione systems in the central nervous system. Antioxid Redox Signal 2017; 27: 989-1010.
[49] Aziz H and Mohiuddin SS. Biochemistry, hexose monophosphate pathway. Treasure Island (FL): StatPearls Publishing; 2022.
[50] Isenmann S, Arthur A, Zannettino AC, Turner JL, Shi S, Glackin CA and Gronthos S. TWIST family of basic helix-loop-helix transcription factors mediate human mesenchymal stem cell growth and commitment. Stem Cells 2009; 27: 2457-2468.
[51] Cao W, Xu C, Li X and Yang X. Twist1 promotes astrocytoma development by stimulating vasculogenic mimicry. Oncol Lett 2019; 18: 846-855.
[52] Li C, Ren Y, Jia X, Liang P, Lou W, He L, Li M, Sun S and Wang H. Twist overexpression promoted epithelial-to-mesenchymal transition of human peritoneal mesothelial cells under high glucose. Nephrol Dial Transplant 2012; 27: 4119-4124.
[53] Geiszt M, Lekstrom K, Brenner S, Hewitt SM, Dana R, Malech HL and Leto TL. NAD(P)H oxidase 1, a product of differentiated colon epithelial cells, can partially replace glycoprotein 91phox in the regulated production of superoxide by phagocytes. J Immunol 2003; 171: 299-306.
[54] Riopel MM, Li J, Liu S, Leask A and Wang R. beta1 integrin-extracellular matrix interactions are essential for maintaining exocrine pancreas architecture and function. Lab Invest 2013; 93: 31-40.
[55] Karamanos NK, Theocharis AD, Piperigkou Z, Manou D, Passi A, Skandalis SS, Vynios DH, Orian-Rousseau V, Ricard-Blum S, Schmelzer CEH, Duca L, Durbeej M, Afratis NA, Troeberg L, Franchi M, Masola V and Onisto M. A guide to the composition and functions of the extracellular matrix. FEBS J 2021; 288: 6850-6912.

[56] Crawford HC, Pasca di Magliano M and Banerjee S. Signaling networks that control cellular plasticity in pancreatic tumorigenesis, progression, and metastasis. Gastroenterology 2019; 156: 2073-2084.
[57] Welgus HG, Campbell EJ, Cury JD, Eisen AZ, Senior RM, Wilhelm SM and Goldberg GI. Neutral metalloproteinases produced by human mononuclear phagocytes. Enzyme profile, regulation, and expression during cellular development. J Clin Invest 1990; 86: 1496-1502.
[58] Choi SH, Kim M, Lee HJ, Kim EH, Kim CH and Lee YJ. Effects of NOX1 on fibroblastic changes of endothelial cells in radiationinduced pulmonary fibrosis. Mol Med Rep 2016; 13: 4135-4142.
[59] Wilkinson-Berka JL, Deliyanti D, Rana I, Miller AG, Agrotis A, Armani R, Szyndralewiez C, Wingler K, Touyz RM, Cooper ME, Jandeleit-Dahm KA and Schmidt HH. NADPH oxidase, NOX1, mediates vascular injury in ischemic retinopathy. Antioxid Redox Signal 2014; 20: 2726-2740.
[60] Pescatore LA, Bonatto D, Forti FL, Sadok A, Kovacic H and Laurindo FR. Protein disulfide isomerase is required for platelet-derived growth factor-induced vascular smooth muscle cell migration, Nox1 NADPH oxidase expression, and RhoGTPase activation. J Biol Chem 2012; 287: 29290-29300.